High-dimensional microbiome interactions shape host fitness

Authors:

Alison Gould,[1*] Vivian Zhang,[1*] Lisa Lamberti,[2] Eric Jones,[3] Benjamin Obadia,[1] Alex Gavryushkin,[2] Jean Carlson,[3] Niko Beerenwinkel,[2] Will Ludington[1]

1. UC Berkeley, Dept Molecular & Cell Biology
2. ETH Zurich, Computational Biology Group, Dept Biosystems Science & Engineering
3. UC Santa Barbara, Complex Systems Group, Dept Physics

* authors contributed equally

Abstract:

With hundreds of species interacting with each other as well as with specific proteins and cells in our body, the gut microbiome is a complex ecosystem embedded within a complex organism. Microbiome impacts on host health can shape key aspects of fitness, such as development,[1] fecundity,[2] and lifespan,[3,4] while the host in turn can shape the microbiome.[5] However, complex interactions between microbes can make impacts unpredictable, such as when toxin-producing *Clostridium* species cause pathogenesis after antibiotics reduce gut diversity.[6] A pressing need exists to deconstruct the effects of gut diversity on host health, and new mathematical frameworks are needed to quantify the high dimensionality of this problem. Central to the microbiome-host relationship are questions of how bacterial diversity is maintained in the gut[7] and how this diversity impacts host fitness.[8] Here we show that interactions between bacteria are major determinants of host physiology and the maintenance of bacterial diversity. We performed a complete combinatorial dissection of the naturally low-diversity *Drosophila* gut microbiome using germ free flies colonized with each possible combination of the five core species of bacteria, forming a discrete 5-dimensional cube in ecological state space. For each species combination, we then measured the resulting bacterial community abundances and fly fitness traits including (i) development, (ii) reproduction, and (iii) lifespan. Notably, we found that the fly gut environment promotes bacterial diversity, which in turn accelerates development, reproduction, and aging. From these measurements we calculated the impact of bacterial interactions on fly fitness by adapting the combinatorial geometry approach of Beerenwinkel-Pachter-Sturmfels[9] (BPS), originally built to measure genetic interactions, to the microbiome.[10] We found that host phenotypes (e.g. lifespan) from single associated bacterial species are not predictive of host phenotypes when in diverse communities. Furthermore, we found evidence that high-order interactions (involving 3, 4 and 5 species) are widely prevalent and impact both host physiology and the maintenance of bacterial diversity, which ecologists have recently predicted.[11] In regard to evolution, the impacts of bacterial interactions on community composition parallel the impacts on host fitness traits, providing a feedback, which, propagated over time, may poise a population for emergence of co-evolving microbiome-host units.

Introduction:

Gut bacteria impact host fitness in beneficial and detrimental ways, for example by improving a poor diet[12-14] or by pathogenesis.[6,15] Identifying specific bacteria responsible for these effects has been difficult, in part due to high gut diversity but also because interactions between bacteria can depend on context, both in terms of neighbor species and the gut environment.[16] For example, a bacterium may produce a specific B-vitamin in response to its neighbors.[17,18] Each microbial response can potentially impact the host, and host feedbacks can mitigate or exacerbate changes in the microbial community.[19] However, vignette examples may be misleading, as the true complexity of a gut microbiome has never been exhaustively quantified. Thus, it remains an outstanding challenge to reverse engineer the interaction networks that characterize community microbiome-host effects relative to single bacterial species microbe-host interactions. Quantifying the set of all possible interactions of n species is a combinatorial problem with 2^n distinct bacterial communities. As n approaches the diversity of the mammalian gut with 100s of species, this problem becomes experimentally intractable.

The fruit fly (*Drosophila melanogaster*) gut microbiome serves as an effective combinatorial model because as few as five species of bacteria consistently inhabit the gut of wild and laboratory flies,[20-22] making 2^5 possible combinations. We first isolated fly gut bacteria in culture, constructed germ-free flies by bleaching the embryos, and reinoculated the newly emerged adult flies via continuous feeding with defined flora using established protocols.[23,24] Here, we made all 32 possible combinations of the five bacterial species commonly found in the fruit fly gut: *Lactobacillus plantarum* (Lp), *L. brevis* (Lb), *Acetobacter pasteurianus* (Ap), *A. tropicalis* (At), and *A. orientalis* (Ao). We quantified the microbiome composition and resultant host phenotypes to determine the relationship between gut microbe interactions and host fitness.

To calculate the complexity of the microbiome-host interactions, we employed mathematical methods which quantify genetic epistasis,[9] i.e. interactions between genetic loci (Box; Math Supplement). By adapting these tools to the microbiome, we draw an analogy between bacterial species and genetic loci,[10] and thereby introduce a logical framework to deconstruct microbiome-host complexity. Our approach is combinatorial in nature, with a distinguishing feature that it considers not only the 26 'standard' interaction tests among five species, but also an additional set of 936 more fine-grained, 'non-standard' interaction tests (Box; Math Supplement). Whereas a standard test in n-dimensions describes a single interaction equation that uses all possible 2^n bacterial combinations (all external faces of the n-cube), our non-standard tests describe many more interaction equations by considering subsets of the complete information (Box; Math Supplement). This enables us to quantify lower-dimensional paths through the high-dimensional microbiome.

Box: Geometric interpretation of species interactions. Like epistatic gene interactions,[9] bacterial species interactions in the fly gut can be described geometrically. To do so we denote by binary strings the species composition. For two species A and B, 00 denotes the absence of both species, 01 and 10 denote the presence of either species A or B, respectively, and 11 denotes the presence of both species. To each such string one associates a phenotype measurement w, for example, fitness. Interaction between the two species can then quantitatively be described by the formula $u_{11} = w_{00} + w_{11} - w_{01} - w_{10}$ measuring deviation from additivity. The interaction is positive if the sum of the phenotypes w_{11} and w_{00} is bigger than the sum of the phenotypes w_{01} and w_{10}.

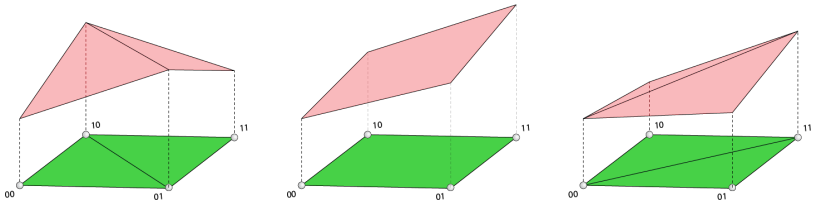

F 1: Geometric interpretation of the interaction between two species.
The vertices 00, 10, 01 and 11 of the blue rectangle represent the four microbiome compositions for two bacterial species. The heights above the points 00, 10, 01, and 11 represent the corresponding phenotypes. A single flat red plane connects the four phenotype points if there is no interaction (**center**), that is, if the phenotype of both species, w_{11}, can be deduced from the phenotypes of the two single species, w_{01} and w_{10}. The figures on the left and right, represent the cases where the interaction is positive (**right**) and negative (**left**). In these cases, the red surfaces connecting the four phenotypes, are divided into two triangular regions, indicating the curvatures of the surfaces.

This geometric approach for describing interactions generalizes to higher dimensions and yields many different quantitative interaction measurements, including standard tests like u_{11} and non-standard tests, which are a broad category using less than the complete number of vertices on the cube (F 2; see BPS[9] and Math Supplement for complete description). Together, these expressions can be used, for instance, to analyze how the non-additivity among a subset of species combinations depends on other bystander species (see Fig S14-S17).

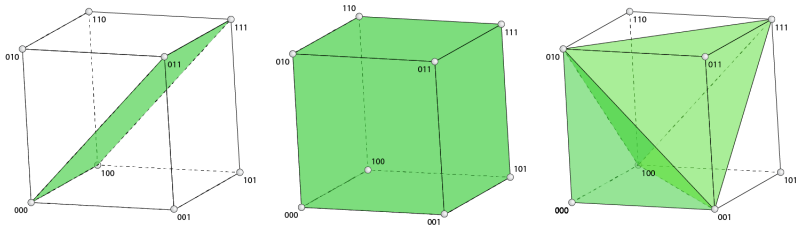

F 2: Geometric interpretation of the standard three species interaction compared with two non-standard interaction tests.
(**Left**) Standard three-way interaction, $u_{111} = w_{111} - (w_{110} + w_{101} + w_{011}) + (w_{100} + w_{010} + w_{001}) - w_{000}$, comparing the phenotypes (not drawn) of all eight bacterial combinations, represented as vertices of the cube. (**Center**) By contrast, the vertices of the blue rectangular region describe a non-standard test, which yields the interaction $g = w_{000} - w_{011} - w_{100} + w_{111}$ involving the phenotypes (not drawn) of the four bacterial combinations 000, 100, 011 and 111. (**Right**) The five vertices of the blue solid bipyramid delineate a non-standard test, $m = w_{001} + w_{010} + w_{100} - w_{111} - 2w_{000}$, derived from a linear combination of other interactions. This particular bipyramid compares the phenotypes (not drawn) of three single bacterial combinations to the combination with all three species and the germ-free case.

Results:

Microbial diversity increases in the intra-host environment

Gut microbiomes support high diversity, which facilitates complexity in the microbiome-host relationship. A classic problem in ecology is how this species diversity persists despite positive feedbacks that tend to destabilize the community.[7] Ecological models suggest that specific patterns of negative species interactions can dampen positive feedbacks to produce stable communities.[7,11] Two related patterns of stabilizing interactions have been proposed, (i) sufficient competition between pairs of bacteria,[7] and (ii) higher-order (more than pairwise) negative interactions that emerge when higher diversity is present.[11]

We first measured the stability of bacterial diversity *in vitro*. We found that *in vitro* culture supported only low diversity,[25] with a maximum of two species coexisting in three rich media types that have a similar composition to fly food. This suggests that simple bacterial interactions do not support diversity (Fig. 1a). However, when we examined the same combinations in the fly gut, high diversity was maintained, up to the complete five species community (Fig. 1a, Fig. S1), indicating that the host environment stabilizes diversity. Diversity significantly increased the total bacterial load (r=0.72, p=3.3E-6, n=32). Average total bacterial load ranged from 165,220 colony forming units (CFUs) per fly for combination 3 (Ap alone) to 702,550 CFUs per fly for combination 28 (Lp+Lb+At+Ao). However, on a species by species basis, abundance stayed constant or decreased (r=-0.43, p=0.050 for Lb; r=-0.50, p=0.047 for Ap; r=-0.84, p=0.0001 for At; p>0.3 for Lp and Ao).

We first quantified species interactions by calculating pairwise correlations in species abundances as a function of the number of species present (Fig. 1b). Correlations became more negative for individual species pairs as diversity increased (p=0.03, n=10, Kendall's Tau checked by Wilcoxon signed rank, see Methods). We used two methods to calculate the directional interactions (i.e. A→B vs. B→A). First, we fit a generalized Lotka-Volterra model and found that bacterial interactions are generally positive when only two species are present (Fig. 1c), suggesting unstable diversity.[26] However, as diversity is increased in the fly, interactions become more negative (Fig. 1c). We directly calculated the same interactions at high and low diversity using Paine's classic approach[27] and found equivalent patterns (Fig. S2), suggesting again that stabilizing interactions emerge as diversity increases, consistent with the theory that high-order interactions support diversity.[11] To specifically test whether high-order interactions occur, we used the BPS[9] framework (see Box). Basing our calculations on the average total bacterial load per fly, we found significant negative high-order interactions by both standard and non-standard tests (Fig S3; Math Supplement), consistent with theoretical predictions.[11]

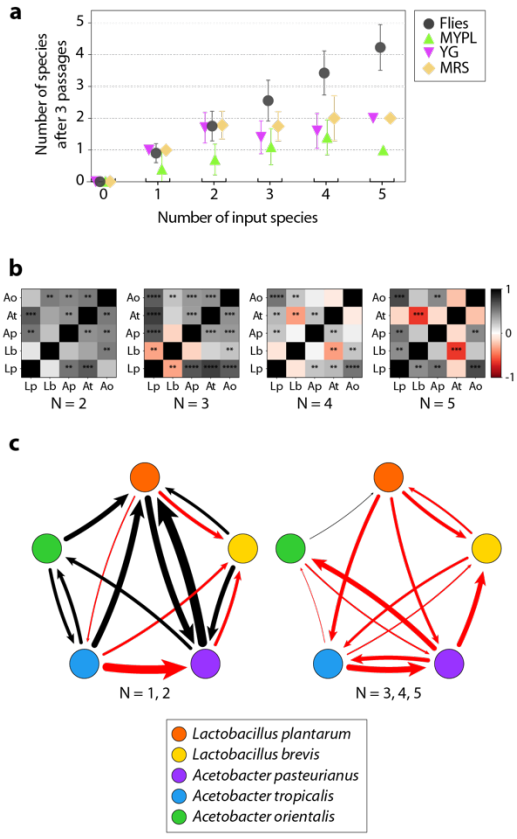

Figure 1. Microbiome interactions stabilize diversity in the fly gut. (**a**) Microbial diversity is maintained inside the fly gut to a greater degree than in liquid coculture. Flies (n=24 per bacterial treatment) were

continuously fed their bacterial treatment (32 total treatments) for 10 days before crushing, plating, and enumerating CFUs (Fig. S1). The same bacterial treatments were inoculated (3 to 6 replicates) into three rich media types that are similar in composition to fly food and passaged 3 times at 48 hour intervals and assayed by plating after the third passage. For all treatments the bacterial diversity displayed is the number of species detected versus the number inoculated. (**b**) Pairwise correlations in abundance for the 5 species of bacteria in fly guts with 2-species, 3-species, 4-species, and 5-species present. More positive correlations are apparent at low diversity, whereas more negative correlations occur as diversity increases ($p=0.03$; see Methods). (**c**) Data were fit to a generalized Lotka-Volterra model to determine the interaction matrix, M (see Methods). Consistent with the correlations in B, more negative interactions occur in more diverse guts (left: 1 to 2 species; right: 3, 4, and 5 species). Direct calculation of interaction strength[27] produced a similar pattern (see Fig. S2).

Microbial diversity preferentially inhibits weak colonizers

The intra-host environment additionally drives probabilistic bacterial colonization in the fly gut,[24] whereas isotropic media lead to deterministic bacterial colonization (e.g. in well-mixed soil[25]). To test how diversity impacts the rate of colonization, we calculated the proportion of flies colonized by each species as a function of the number of species fed (Fig. S4a). Lp and Ao colonized at nearly 100% independent of background diversity, whereas Ap and At (and to a lesser extent Lb) colonize at a lower rate as diversity increases. This pattern changed when the input of new bacteria was terminated by transferring flies continuously to fresh food (Fig. S4b). Ap in particular colonized better in more diverse guts, suggesting that bacterial interactions may aid Ap populations. The diversity-dependent colonization load is consistent with niche processes of competitive exclusion:[24,28] as diversity increases, the available niches are more likely to become occupied by a strong colonizer (e.g. Lp or Ao), subsequently inhibiting weaker colonizers (e.g. Lb or At).

We note that the limit of detection (~1000 CFUs) may mask low abundance colonization. While the limit of detection did not impact the analysis of bacterial interactions (Fig. 1b,c; Math Supplement), additional analysis of colonization of individual flies by plating indicated that many flies, which appear uncolonized, were in fact colonized at levels below the limit of detection.[24]

Microbial diversity accelerates development

We next investigated what effect gut diversity has on host fitness traits. The time an egg takes to develop into an adult influences fitness because faster development reduces generation time.[29] On our replete food, both germ-free and flies colonized with all 5 bacteria species have a ~10 day development rate (Fig. 2a). We hypothesized that fly development would be relatively robust to changes in bacterial composition. However, as we dissected the 5-member bacterial community, we observed faster development rate with increasing bacterial diversity (Fig. 2a; Fig. S5; $r=-0.48$, $p=0.006$, $n=32$, Pearson coefficient). The overall decreased development rate demonstrates that higher gut diversity can increase fly fitness.

Bacterial food conversion drives development rate

We hypothesized that changes in fly development are primarily nutritional and therefore due to changes in total bacterial load rather than individual species.[30] Because gut bacterial abundance correlates with food bacterial abundance in flies,[31] we compared the adult bacterial load with each of the physiology phenotypes (Fig. S6). We found a significant negative correlation between bacterial load and development rate (indicating faster development; $r=-0.52$, $p<0.005$), indicating that bacterial interactions influence some aspects of host physiology through total bacterial load.

The link between juvenile development rate and adult bacterial composition could be influenced both by bacterial populations in the food and by parental effects. To differentiate these hypotheses, we performed two experiments. First, we quantified bacterial load in the fly food (Fig. S7). Significantly fewer bacteria occurred per mg in fly food than in the gut of adult flies (p=1.3E-8, n=16, paired sample t-test), but there was a significant correlation between total bacterial abundance in fly food and in fly guts (r=0.80, p=2.3E-4, n=16, comparing matched bacterial combinations) as previously reported.[31] However, in contradiction to the prediction that bacterial load drives development rate, there was no correlation between food bacterial abundance and development rate (r=0.018, p=0.95, n=16 for total CFUs). On an individual species basis though, Ao abundance was correlated with development rate (r=-0.89, p=0.0095, n=7 for Ao CFUs). However, there was no correlation with the other fly physiology parameters measured, suggesting that a single species, Ao, influences development rate in the larval stage.

We next tested whether there was a maternal effect on development rate by removing the maternal bacterial association. We harvested eggs from germ-free flies and associated them with all 32 bacterial combinations. This experiment showed insignificant differences in development rate compared with the experiment with gnotobiotic females, indicating that maternal effects do not set developmental timing (Fig. S8). In contrast, heat-killed duplicates of the experiment showed significantly slowed developmental pace (p<0.005, n=16, paired sample t-test), suggesting that active bacterial metabolism[32] is important for fly development (Fig. S8). From a fitness perspective, these results indicate that female flies gain an advantage for their offspring by associating with these diverse bacterial consortia.

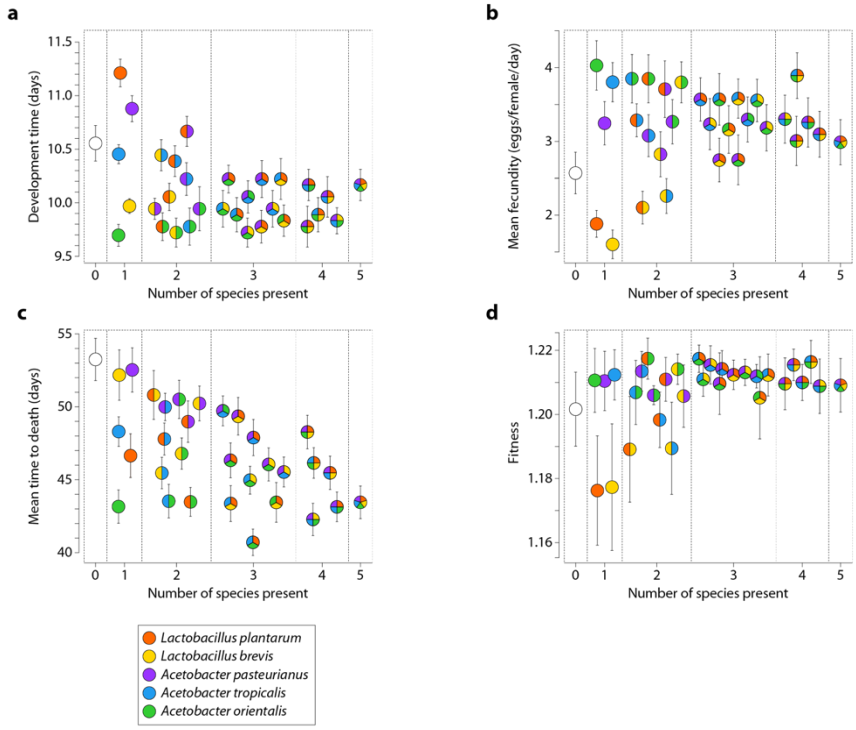

Figure 2. Microbiome diversity impacts host physiology. (**a**) The number of days to adulthood was measured as the first pupa to emerge from fly vials changed out every three days during the lifespan experiment. The development rate increases as gut diversity increases. Median n=24 per bacterial treatment (see Fig. S5). (**b**) Mean fecundity per female per day was measured concomitantly with development rate over the flies' lifespans. Median n=65 vials measured per bacterial treatment. Variation in fecundity decreases as gut diversity increases (Fig. S5, S9). (**c**) Lifespan decreases as gut diversity increases. Median n=100 flies per bacterial treatment (Fig. S5, S10). (**d**) Fitness calculations using a Leslie matrix populated with data from **a-c** reveals an increase in fitness and a decrease in variation as gut diversity increases.

Variation in fly fecundity decreases with increasing diversity

Fitness is closely tied to fecundity, the number of viable offspring produced by an individual. We counted the number of adult progeny produced per fly over its lifespan and found that overall, average fecundity did not vary as a function of increasing biodiversity (r=0.072, p=0.70, n=32, Pearson coefficient) or bacterial load (r=0.082, p>0.05, n=32, Pearson coefficient; Fig. S5, S9). However, the variance in fecundity between bacterial combinations with the same number of species decreased as species were added (Fig. 2b, S9; r=-0.91, p=0.08, n=4 diversities, Pearson coefficient; p=0.001, t-test comparing deviations with 1 or 2 species vs. 3 or 4), indicating that diversity decreases the risk of low fecundity.

Germ-free flies live longer than flies colonized by bacteria

In 1927, Steinfeld[3] showed that germ free flies live longer than their microbially-colonized counterparts. This result that the microbiome can impact aging has been replicated in flies and vertebrates.[4,33] Consistent with these previous studies, our germ-free flies survived longer than flies colonized with all 5 species of bacteria (mean lifespan ± s.e.m. was 53.5 ± 1.5 germ-free vs. 43.5 ± 1.1 for 5 species gnotobiotics). Examining fly survival as a function of increasing gut diversity, we found a decrease in survival over many different bacterial associations (Fig. 2c, S5, S10; r=-0.54, p=0.002, n=32) and as a function of bacterial load (r=-0.47, p<0.005). The trend of decreased lifespan corresponds to an increase in fecundity (average daily fecundity vs. lifespan: r=-0.50, p=0.003, n=32; Fig. S11a) and is not explained by differences in fly activity (Fig. S12). Such life history tradeoffs are well-documented in the literature and are believed to constitute a differential allocation of resources between long term body maintenance and reproduction.[29,34] This suggests the tradeoff may be inherent and that high reproduction and long life are mutually exclusive.

To examine this hypothesis, we used antibiotics to remove the microbiome of high fecundity flies and measured the resulting change in lifespan for female flies. We first allowed flies with the high fecundity microbiomes to reproduce for 21 days (to a level greater than total lifetime fecundity of germ-free flies), and we subsequently eliminated the microbiome using antibiotics. In general, the midlife elimination of gut flora lengthened fly lifespan by roughly 15% compared to flies continuously fed live bacteria (p=0.007, n=7, paired sample t-test, Fig. S11b), without decreasing total fecundity (p=0.2, n=7, paired sample t-test, Fig. S11b). This result demonstrates that the life history tradeoff is not necessarily fixed and suggests that flies choose rapid and high fecundity in response to a perceived risk of death due to microbes. However, two specific bacterial combinations showed no increase in lifespan when given antibiotics, Ao and Lp+Lb+Ao. Very similar microbiome compositions showed significant lifespan extension (e.g. Lp+Ao and Lp+At+Ao), demonstrating the complexity of the microbiome-host relationship. When we performed the reverse experiment and associated midlife germ-free flies with high fecundity bacteria, there was a significant increase in fecundity and a significant decrease in lifespan (p=0.007, n=4, paired sample t-test for fecundity; Fig. S11b; p=0.006, n=4, paired sample t-test for lifespan), consistent with our initial experiments (Fig. 2), and indicating that the life history tradeoff is dynamic throughout life.

Microbial diversity increases host fitness

We wondered how the lifespan-fecundity tradeoff impacted organismal fitness, which is defined as the rate of population growth. To address this question, we combined our data for development, fecundity,

and lifespan in the Leslie matrix,[35] a classical model of population growth, to calculate organismal fitness under each bacterial association. Overall, fitness was relatively consistent across different bacterial associations (Fig. 2d). However, the variation between low diversity microbiomes fitness was higher than between high diversity microbiomes, indicating that the life history tradeoff is more effective at high diversity.

Microbial interactions impact host fitness

Previous studies of complex microbiomes have suggested that interactions among species drive impacts on the host. For example, *Clostridium difficile* pathogenicity induction is repressed by the presence of other species.[6] Alternatively, interactions may be mediated by the host: gut colonization by a specific *Escherichia coli* strain can induce tolerance to *Burkholderia* infection in the lungs mediated by IGF-1.[15] Our data suggest complex interactions between bacteria with impacts on host physiology. For instance, flies mono-colonized with Lp, At, or Ao have mean survival times of 47, 48, and 43 days respectively. No significant changes occur with pairs of species, but fly survival drops to 41 days when all three bacteria are inoculated together. To determine whether the interaction is of high order compared to the alternative hypothesis that pairwise interactions can explain the three species phenotype, we applied the mathematics of epistasis (Box),[9] which was originally developed as a framework to calculate interactions between genes in high dimensions. Here we generalize the method to characterize high-dimensional interactions in the microbiome.

We used this epistasis framework to calculate the interactions between gut bacterial species and their impacts on host physiology (Math Supplement). Notably, the effects on host physiology could not be attributed to simple changes in individual species abundances, aside from the development rate of 7 samples containing Ao as noted previously. Instead, we found significant effects of species interactions on host physiology and total bacterial load (Fig. 3a-d, S3), with wide prevalence of non-additive pairwise and high-order interactions. Interestingly, development rate interactions tend to be negative. Negative epistasis in genetics suggests the two loci are in the same pathway, i.e. they are redundant. By analogy, negative microbiome epistasis in development rate suggests redundant mechanisms, such as nutrition,[30] confer microbiome effects on the host. In contrast, time to death interactions tend to be positive, suggesting that bacterial interactions synergistically modulate different pathways. CFUs and fecundity (Fig. 3e-h) both show significant positive and negative interactions, suggesting both synergy and redundancy. The magnitudes of the interactions, when normalized to the number of species present, are often as large as the effects of individual species introductions, indicating that the species interactions are as important as the presence of the species themselves (Math Supplement). Thus, changes in gut microbiome composition impact host physiology in non-additive ways.

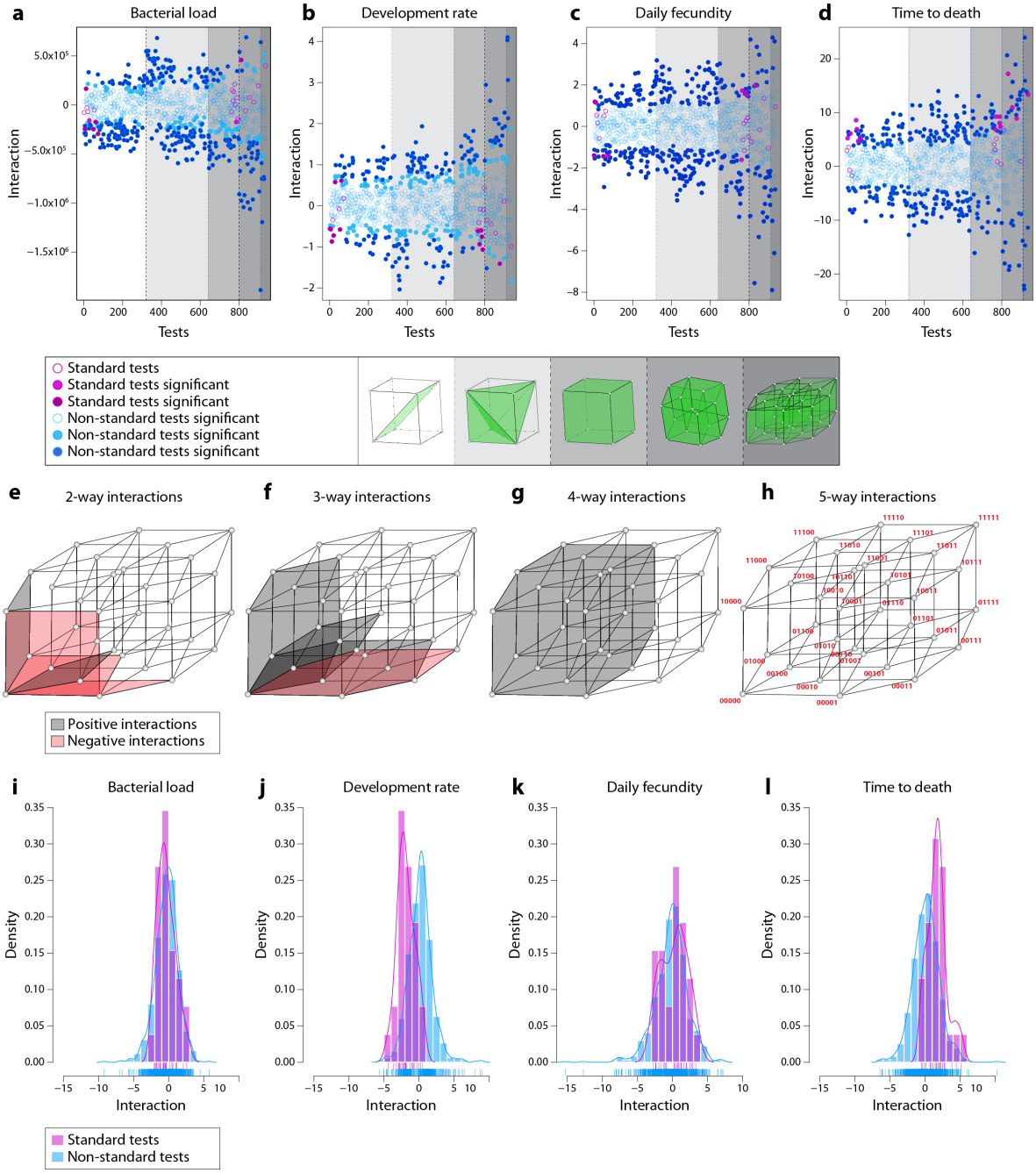

Figure 3. Microbial interactions drive the microbiome-host relationship. (**a-d**) Interactions become stronger as diversity increases. For (**a**) bacterial load, (**b**) development, (**c**) fecundity, and (**d**) time to death, we calculated the interaction coordinates for standard tests (pink dots) and non-standard tests (blue dots) for phenotype data (Fig. 1,2). Filled circles: significant interactions; open circles: non-significant interactions. See Fig S13 for standard tests with species identities. (**e-g**) Standard interaction coordinates for fecundity (panel **c** and Fig. S13) are depicted on the 5-cube significant positive interactions (gray) vs. significant negative interactions (red). (**h**) No significant 5-way interaction occurs for fecundity. Bacterial combinations are indicated in binary as the vertices of the 5-cube. (**i-l**) Comparisons between the distributions of standard and non-standard interactions show significant shifts, indicating context-dependence of the interactions due to bystander species. To provide a visual comparison of interaction strengths between the phenotypes, raw data were first normalized (z-scores) and then interactions were calculated.

Complexity in the microbiome could arise due to context-dependent effects, where two species interact differently depending on the presence of a third. We found a large dependence on context by calculating how interactions change in the presence of bystander species. The "non-standard tests" we computed (see Box; Math Supplement) are adaptations of generally known interaction tests called marginal and conditional epistasis in genetics. Comparing these non-standard tests to the standard ones provides a quantitative measure of context-dependence. We found significant context-dependence (Fig. 3i-l; Fig. S14-S17; Math Supplement), indicating that low-dimensional interactions are significantly changed by the addition of bystander species. Thus, the dimensionality of the microbiome is high, and the impacts of individual species vary greatly according to their co-inhabitants of the gut. However, in some specific cases where a standard test indicated epistasis, certain related, non-standard tests of the same bacterial species interactions indicated additivity (Fig. S14-S17). Therefore, our methods reveal lower dimensional routes to additively traverse the high-dimensional microbiome landscape (Fig. 3a-d; Math Supplement Fig. S5-8). While we found no consistent interaction patterns to infer these routes *a priori*, the results suggest a path to predictability if we can discover rules of these low-dimensional interactions on the high-dimensional landscape.

From an evolutionary perspective, many reports document host-specialized microbiomes with a phylogenetic signature and correlated fitness consequences of this co-adaptation.[36-39] We observed no relationship between host fecundity and bacterial abundances (Fig. S6a), suggesting that the microbiome-host unit may not necessarily select more fit individuals nor favor cohesive group selection.[10,40] Rather, we see a significant relationship between the bacterial interactions generated by bacterial abundance and host fecundity phenotypes (Fig. S6b-d), indicating that microbiome epistasis shapes community structure and that this structure similarly shapes host fitness. The high level of epistasis in the community landscape and correlated epistasis in host fitness traits suggest that differences in microbiome diversity between hosts may be stable[24,41] and have phenotypic consequences (Fig. 2), which increases standing phenotypic diversity in a population of hosts, priming hosts and their microbiomes for divergent selection but not causing it. We propose correlated epistasis between microbiome ecology and host fitness as a mechanism that poises a microbiome-host system for formation of specialized gut communities.

Materials and Methods

Fly stock maintenance: *Wolbachia*-free *Drosophila melanogaster* Canton-S flies were reared on a cornmeal-based medium (6.67% cornmeal, 2.7% active dry yeast, 1.6% sucrose, 0.75% sodium tartrate, 0.73% ethanol, 0.68% agar, 0.46% propionic acid, 0.09% methylparaben, 0.06% calcium chloride, and 0.01% molasses). Fly stocks were maintained at 25˚C, 60% humidity, and 12:12 hours light:dark cycles. Fly stocks were tested for the presence of known RNA viruses by RT-PCR and in this regard were virus-free.[24] Germ-free fly stocks were kept in sterile conditions over multiple generations to reduce any heterogeneity due to parental nutrition derived from microbiome variability.

Germ-free fly preparation: *Wolbachia*-free and virus-free *Drosophila melanogaster* Canton-S flies reared on a cornmeal-based medium were transferred to embryo collection cages and allowed to acclimate in the cage for at least one day before egg collection. On the morning of egg collection, a yeast paste was added on a grape juice agar plate. Flies were left to lay eggs on this grape juice agar plate for 5-6 hours. Eggs were then collected into a 0.4 μm cell strainer. In a biosafety cabinet, fly eggs were rinsed twice in 10% bleach (0.6% sodium hypochlorite) for 2.5 min each, once in 70% ethanol for 30 seconds, and three times in sterile dH_2O for 10 seconds each. Approximately 50 eggs were transferred to sterile fly media (10% glucose, 5% active dry yeast, 1.2% agar, 0.42% propionic acid) with a sterile cotton swab.

Bacteria strains: *Lactobacillus plantarum*, *L. brevis*, *Acetobacter pasteurianus*, *A. tropicalis*, and *A. orientalis* bacteria were isolated from *D. melanogaster* lab flies. Bacteria were grown overnight in MRS media in a shaker set at 30˚C. The bacteria were resuspended at a concentration of 10^8 cells/mL in sterile PBS for fly gnotobiotic preparations[23] so that constant numbers of CFUs were inoculated per fly vial. The 32 combinations of the 5 bacterial strains were mixed using a Beckman Coulter Biomek NXP workstation to standardize the inoculum. Vials were swabbed to ensure correct bacterial species were present and no contaminants.

Adult gnotobiotic fly preparation: Germ-free flies aged 5-7 days were sorted into 10% glucose, 5% active dry yeast medium inoculated with a defined mixture of bacteria. Each vial contained a total of $5x10^6$ CFUs (50 μL of 10^8 bacteria/mL). Ten female and ten male flies were transferred into each vial. Gnotobiotic flies were flipped into freshly inoculated media every 3 days.

Concurrent lifespan assay, fecundity (pupae counts), fly development (Fig 2a-c): We measured all host fitness phenotypes concurrently in mixed sex populations in order to mimic more natural conditions. To measure the lifespan of flies on each combination of bacteria, we recorded the number of flies living and number of flies dead daily until the entire population was dead. Dead flies were removed when the vials were flipped. Average daily female fecundity was assessed by counting total amount of pupae in each vial after the adults were flipped to a fresh vial. Due to the variable developmental times involved, vials were monitored daily for 14 days after removing the adults.
As part of this experiment, we counted the day when the first adult emerged from each vial. We chose this metric because adults were housed in the same vial for 3 days and therefore the start of development was not synchronized.

Development Assays (Fig. S8): In the experiments presented in Fig. S8, development times were assessed for each egg introduced to the vial. Eggs were first dechorionated and sterilized as in *Germ-Free Fly Preparation section*. Eggs were then suspended in 1x PBS with 0.1% TritonX detergent to allow

pipetting of the eggs. Roughly 30 eggs [and always >20] were pipetted into the recipient vial. Timing of pupation and eclosion in vials that flies had previously developed in was assayed at one day intervals for non-heat-killed (blue dots) and heat-killed (red dots) vial preparations. For the germ-free eggs inoculated with fresh bacteria (Fig. S8 black points) developmental timing was assessed at ~3 hour intervals.

Bacterial load counts (Fig. S1): To assess the number of colony forming units (CFUs) per fly, flies were washed in 70% ethanol for 5 seconds, rinsed in ddH_2O for 5 seconds, and then put into the well of a 96-well plate containing 100 μL PBS and 80 μL 0.5 mm glass beads. Plates were heat sealed with aluminum sealing film then beat beaten for 60 seconds at maximum speed in a MiniBeadBeater-8 converted to hold a 96-well plate using a custom-built attachment. Plates were then pinned with a 96-pin replicator (Boekel) in three technical replicates per fly onto selective media that allowed us to visually distinguish each bacterial species. Selective media are as follows: MRS with X-gal grows only Lp and Lb within 2 days. Lb colonies turn blue while Lp colonies remain yellowish-white. MYPL with 5 mg/L tetracycline grows only Ap and Ao. MYPL with 50 mg/L gentamycin grows only At and Ao. The flat Ao colonies with a distinct ruffled border are easily visually distinguished from the rounder, thicker, and browner Ap and At based on colony morphology.

Locomotion assay (Fig. S12): Gnotobiotic flies were prepared as previously described. Ten females and ten male flies were sorted into each vial. Each vial was flipped every 3 days into media inoculated with its bacteria mixture. After the 9th days (the third flip), gnotobiotic flies were flipped into a vial containing sterile media (10% glucose, 5% yeast, 1.2% agar, and 0.42% propionic acid). These vials were placed into the LAM25 (Locomotor Activity Monitor) kept in 25˚C, 60% humidity, and 12 hour light: 12 hour dark cycles and monitored for 7 days.

Fitness calculations (Fig 2d): Estimated fitness per vial within treatment using Leslie matrix (1,000x per treatment). For each replicate Leslie matrix, we randomly sampled from the experimental replicates of development time data per treatment. Female fecundity was counted as zero until the day of adult emergence. Thereafter, the fecundity was filled from the data by random sampling of the 5 different replicates for each time point.
The diagonal was filled with "1"s corresponding to the development time. After development, the adult survival data was used, by randomly sampling the 5 adult survival probability replicates for each day. The remaining values in the matrix are zeros. We then calculated the dominant eigenvalue of the matrix for each of the 1,000 replicate samplings, giving us a range of fitness estimates. This fitness value, λ, corresponds to the daily fold expansion of the population, $n_{t+1} = \lambda n$, under ideal conditions.

Statistical analyses: All statistics were calculated using R unless otherwise noted. Survival data average curves were calculated as the cumulative proportion of the population that died over time. A 2-parameter Gompertz function was selected using the 'drc' package in R (v.3.3.3), $n(t) = e^{-e^{-a(t-b)}}$, where $n(t)$ is the proportion of the population surviving as a function of time. The same approach was applied to fit the fecundity data, resulting in a 3-parameter Gompertz model selected by the Akaike information criterion, $f(t) = f_0 e^{-e^{-a(t-b)}}$.

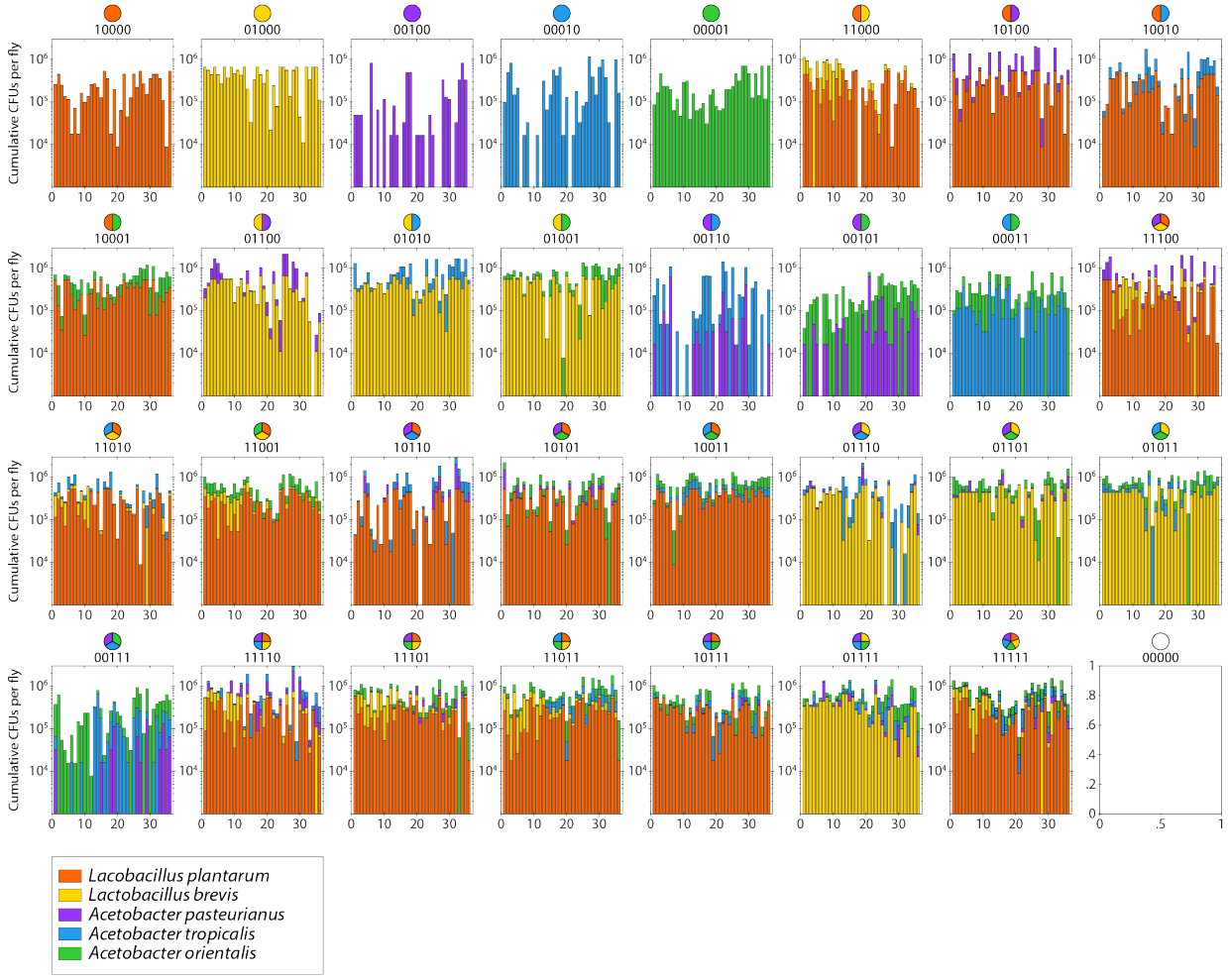

Figure S1. Representative raw bacterial abundance counts (CFUs) for each fly with each bacterial combination. X-axes indicate individual flies. Y-axes are CFUs on a $\log_{10}$ scale. Color scheme indicates species identity consistent with Fig 1c. For each bacterial combination, the first 12 flies are from a treatment where flies were fed defined bacteria continuously for 10 days and then transferred daily to fresh food for 5 days. The last 24 flies for each bacterial combination are for the treatment where fly development, fecundity, and time to death were measured (Fig 2). Note that there are subtle differences between the first 12 and last 24 flies for some bacterial combinations (e.g. Ap+At+Ao). These differences are quantified in Fig S3a versus S3b.

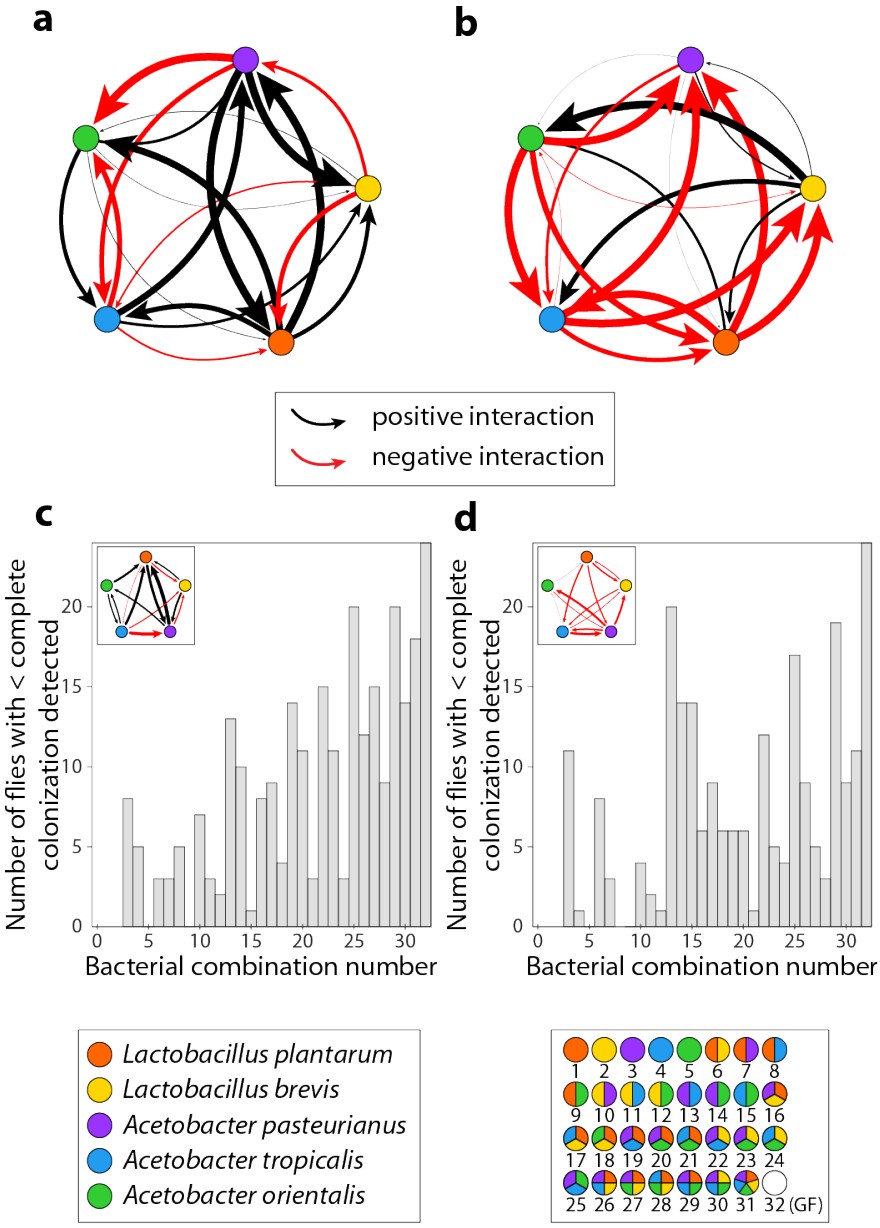

Figure S2. Pairwise bacterial interactions in the fly gut transition from positive to negative as diversity increases. Direct interaction strength was calculated per Paine[26] as noted in Math Supplement. Average microbial abundances across replicates were used. (**a**) Interactions calculated by comparing treatments with two species to treatments with one species. (**b**) Interactions calculated by comparing the treatment with five species to the treatments with four species. (**c**) Number of flies where not all inoculating bacteria were detected (1,000 CFUs limit of detection) for each bacterial combination when flies were continuously fed bacteria. (**d**) Number of flies where not all inoculating bacteria were detected (1,000 CFUs limit of detection) for each bacterial combination when flies were daily transitioned to germ-free food for 5 days after an initial 10-day continuous inoculation period.

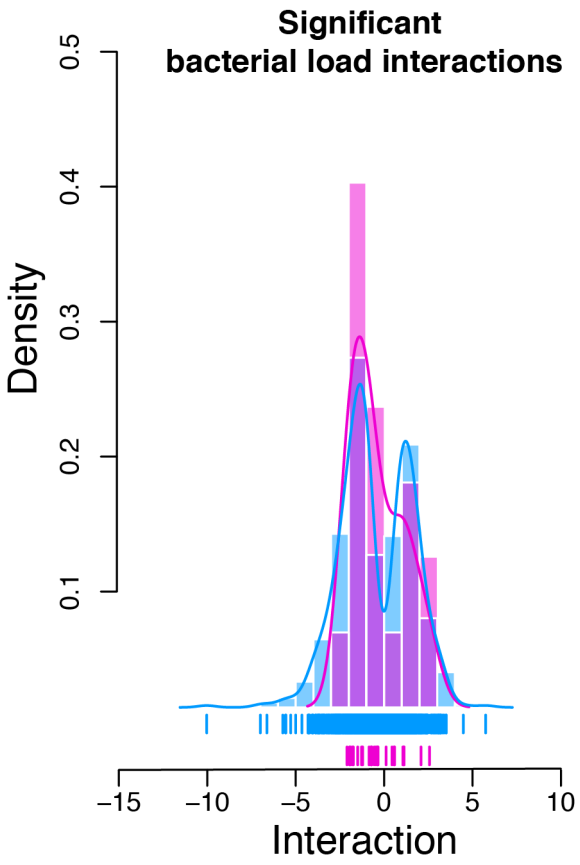

Figure S3. Microbial interactions drive the per-fly bacterial load. Standard interactions (pink) and non-standard interactions (blue) are both show significant densities of non-zero scores. Mean total bacterial abundance from each bacterial combination (n=24 flies continuously fed bacteria, same raw data used as in Fig 1b) was calculated and converted to a z-score. Interactions were calculated for all 26 standard tests and 910 non-standard tests (Math Supplement). Histograms of interaction scores (large vertical bars) were converted to a probability density function (smooth curve) using a Gaussian kernel. Actual scores are shown below the histograms (short vertical lines).

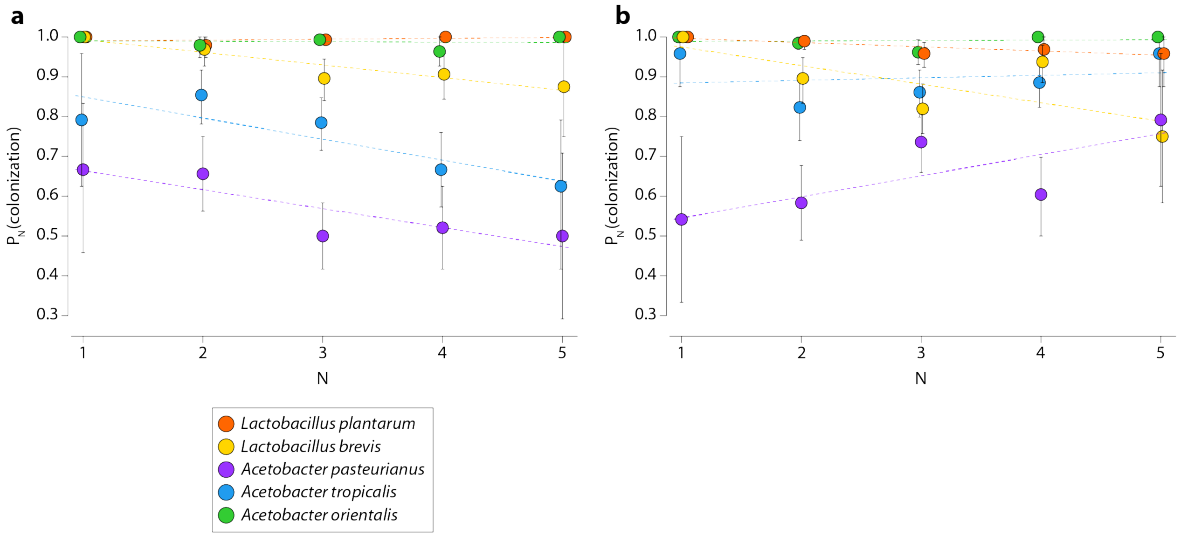

Figure S4. Higher gut diversity decreases the proportion of colonized flies for weak colonizers. (**a**) Flies continuously fed on food colonized with a high bacterial load show a decrease in the likelihood of detecting colonization for certain species (1,000 CFUs limit of detection). Ap, At, and to a lesser extent Lb showed lower likelihood to colonize as total diversity increased. Lp and Ao showed complete colonization across a gradient of species diversity. (**b**) This change in colonization likelihood shifted when we flipped flies daily to fresh food for five days after an initial 10-day colonization by continuous inoculation. Notably, Ap colonization likelihood increased with increasing diversity when we removed the bacterial supply, suggesting Ap is a better competitor than it is a colonizer.

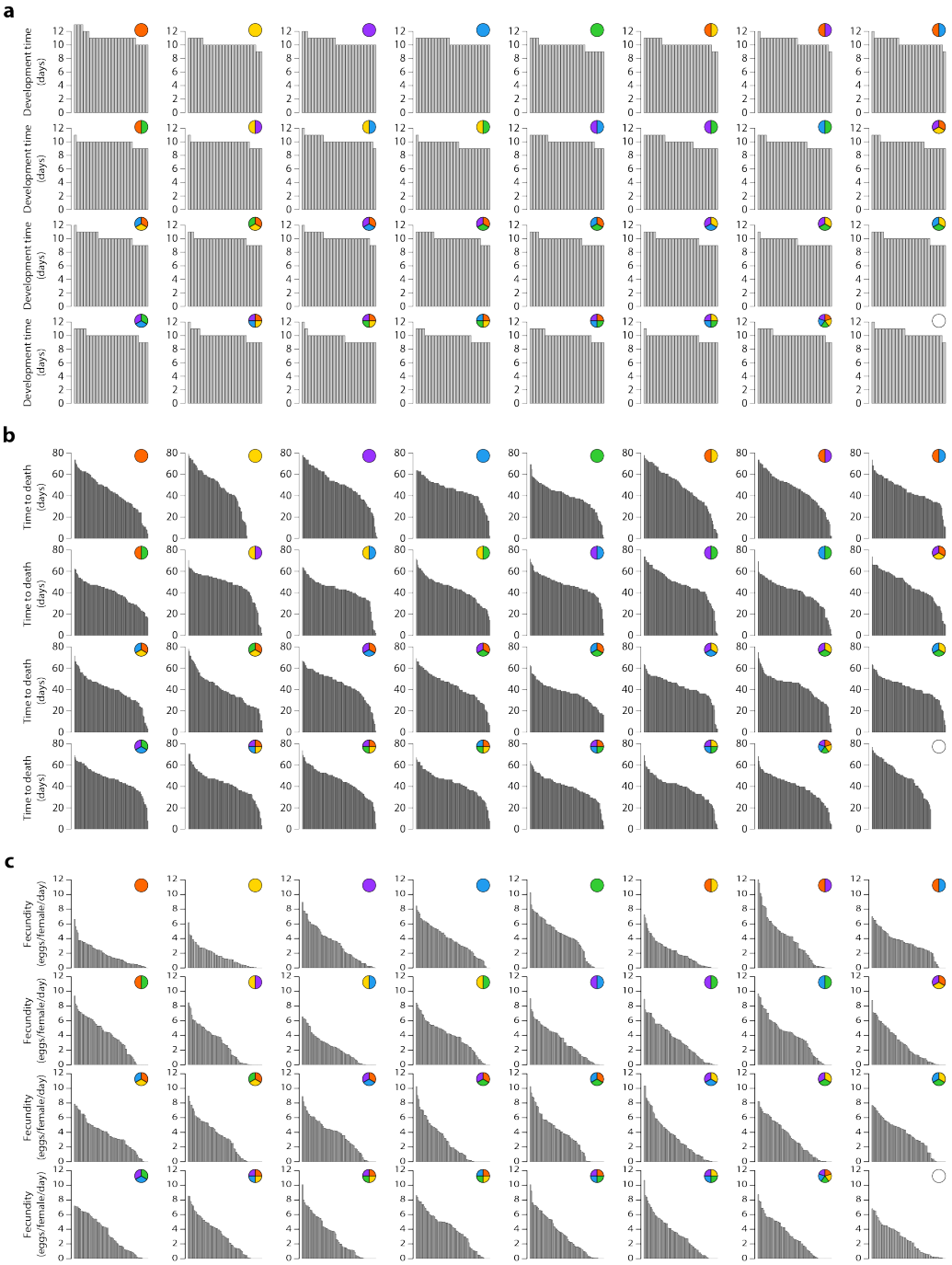

Figure S5. Raw data from development rate, fecundity, and time to death. (**a**) Development time raw data by microbial treatment. Each bar within a treatment is the fastest developing fly within a vial. (**b**) Time to death raw data by microbial treatment. Each bar represents the lifespan of an individual fly. Male and female flies are aggregated as no statistically significant difference could be detected between male and female lifespans in these mixed sex experiments. (**c**) Fecundity per day per female raw data by treatment. Each bar represents the total fecundity measured from a single fly vial normalized to the number of adult female flies.

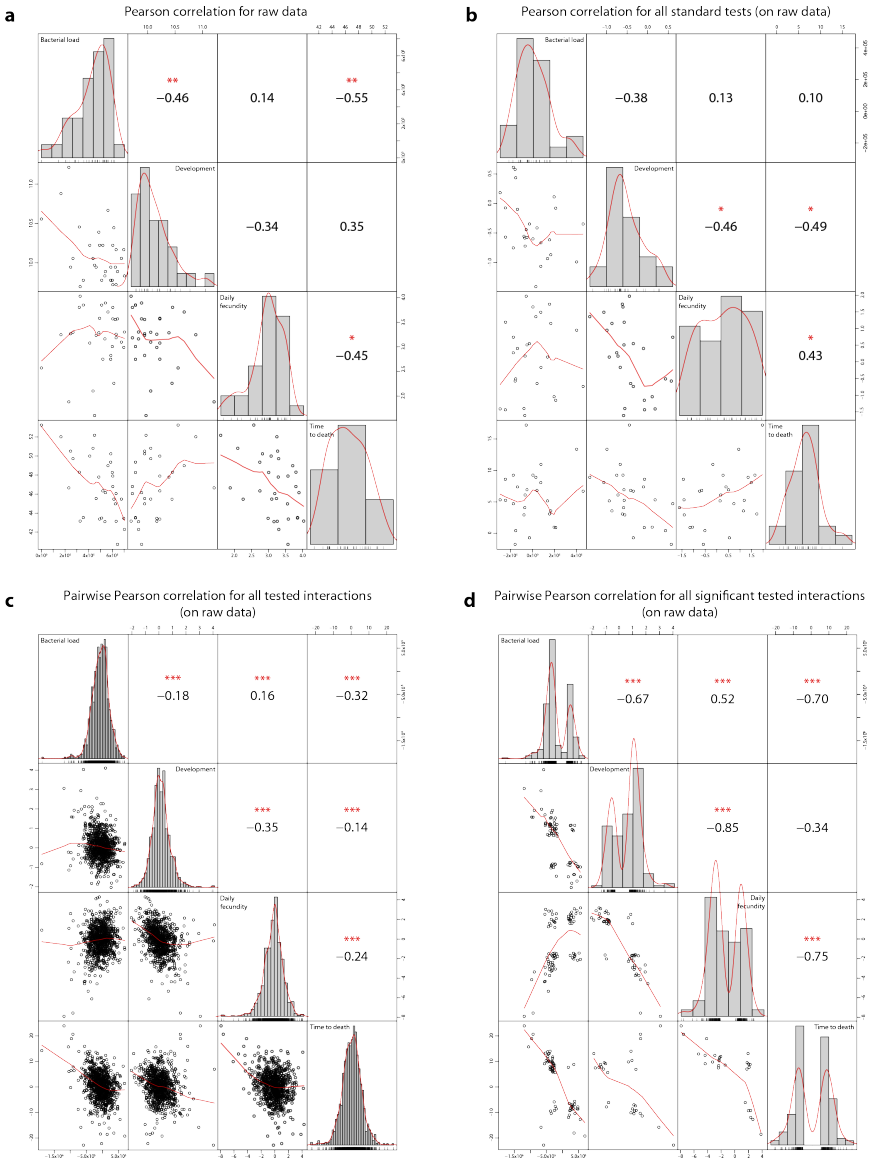

Figure S6. Pearson correlation of raw phenotypes and interactions. (**a**) Raw data correlations between measured host and bacterial phenotypes indicates significant relationships between phenotypes except between fecundity and total gut CFUs. (**b**) Pearson correlation of all standard interaction strengths between measured host and bacterial phenotypes indicates significant relationships between the three different host phenotype interactions but no significant relationship between total gut CFUs and any of the host phenotype interactions. (**c**) Pearson correlation of interaction strengths for all standard and non-standard tests indicates significant relationships between all phenotypes. (**d**) Pearson correlation of only significant interaction strengths after multiple comparisons correction (standard and non-standard tests) between measured host and bacterial phenotypes indicates significant relationships between all phenotypes. Scatter plots below the diagonal. Histograms on the diagonal. Correlation coefficients and significance values (* indicates p<0.005; ** indicates p<0.001; *** indicates p<0.0001) above the diagonal.

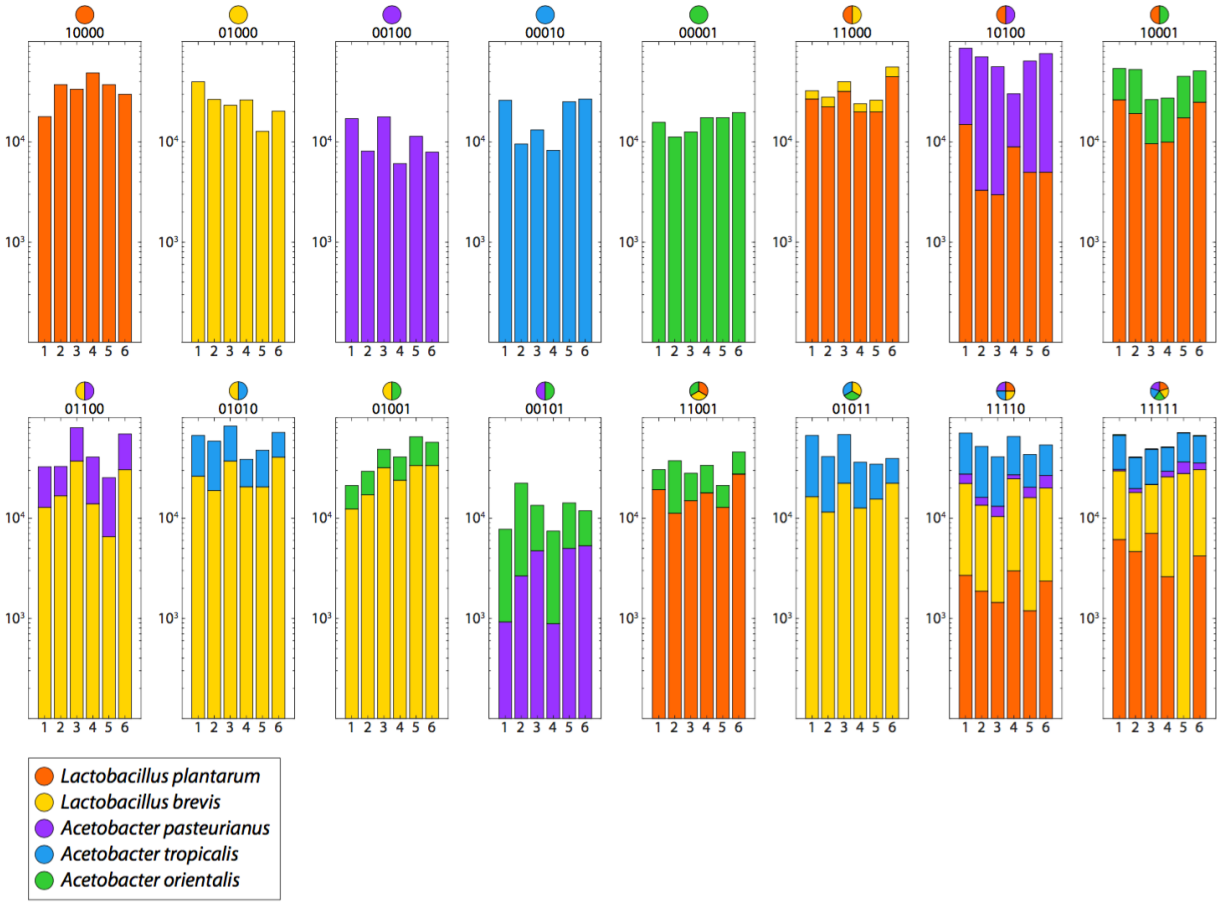

Figure S7. Raw bacterial abundance counts (CFUs) for fly food treatments with 16 selected bacterial combinations. X-axes indicate individual food samples 1 to 6. For each combination, the first three samples are from the first biological replicate, and the last three are from the second biological replicate. Y-axes are CFUs on a Log_{10} scale. Color scheme indicates species identity consistent with Fig 1c.

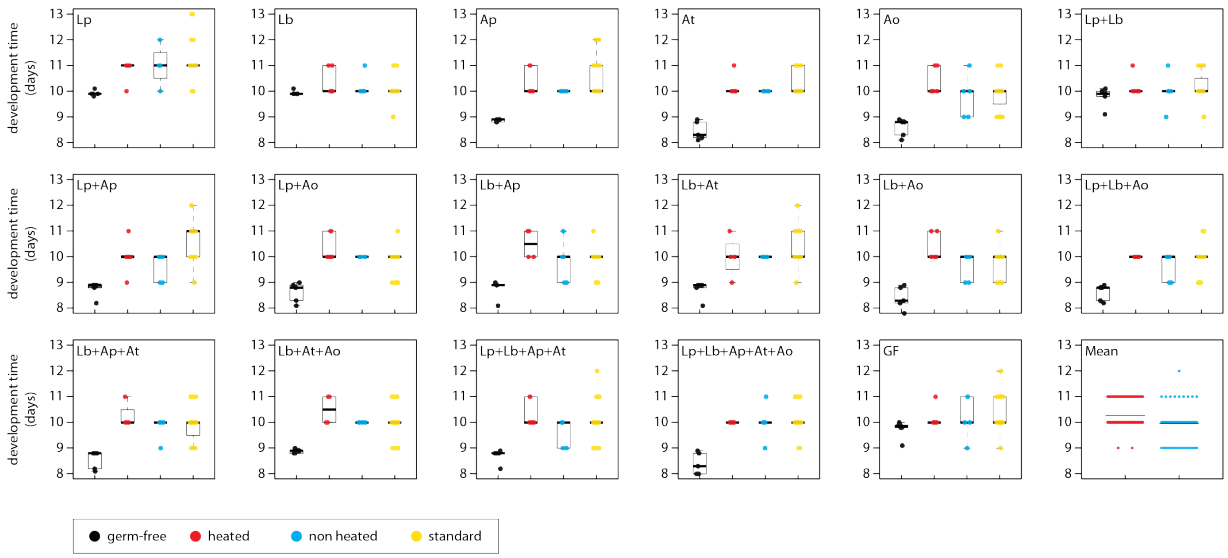

Figure S8. Parental effects and live bacteria influence offspring developmental pace. 16 different microbial combinations and germ-free flies (same as in Fig. S7) were tested for their impacts on developmental pace (number of days from egg laid to adult emergence from pupal case). In the original experiments, the developmental pace was measured for flies where eggs were directly laid by females continuously inoculated with their bacterial combination. To test the role of parental effects, we experimentally varied the source of the eggs as well as the bacterial treatment. Bacterial combination is indicated above each plot. Black points show data for n=20 eggs taken from germ-free mothers. Yellow points show the standard data (Fig. 2a) as a reference. Blue points show data where colonized vials (with flies and bacteria) were emptied of all their flies (and larvae) and then n=20 germ free eggs were introduced. No significant differences were detected between yellow and blue treatments. Red points show data where the treatment was identical to the blue points except that the vials were heat-killed of bacteria at 60˚C for 1 hour (and tested for sterility) prior to germ-free egg introduction. This treatment significantly increased the development time (see main text). The fastest development times were for eggs introduced to fresh vials inoculated with bacteria but without previous fly occupation. In this final treatment (black dots) there was very little variation between treatments except that flies lacking all *Acetobacter* species were delayed by 1 to 2 days with respect to their cohort.

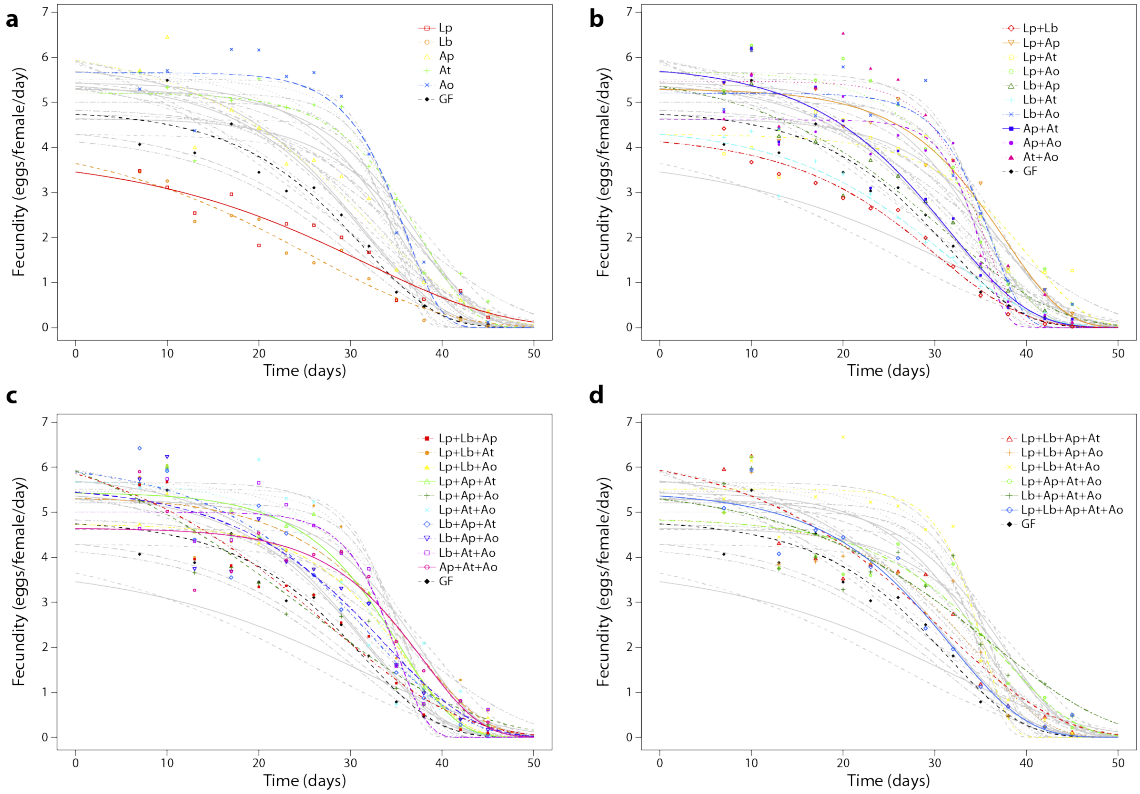

Figure S9. Curve fits to raw fecundity data aggregated from all 5 experimental replicates for each bacterial combination. Curve fits to a 3-parameter Gompertz distribution are depicted (see Methods). Bacterial combinations are grouped by the number of species. (**a**) Single species and germ-free flies. (**b**) Species pairs and germ-free flies. (**c**) Species trios and germ-free flies. (**d**) Species 4-way combinations, 5-way combination, and germ-free flies. All [grayscale] curves are kept as a reference.

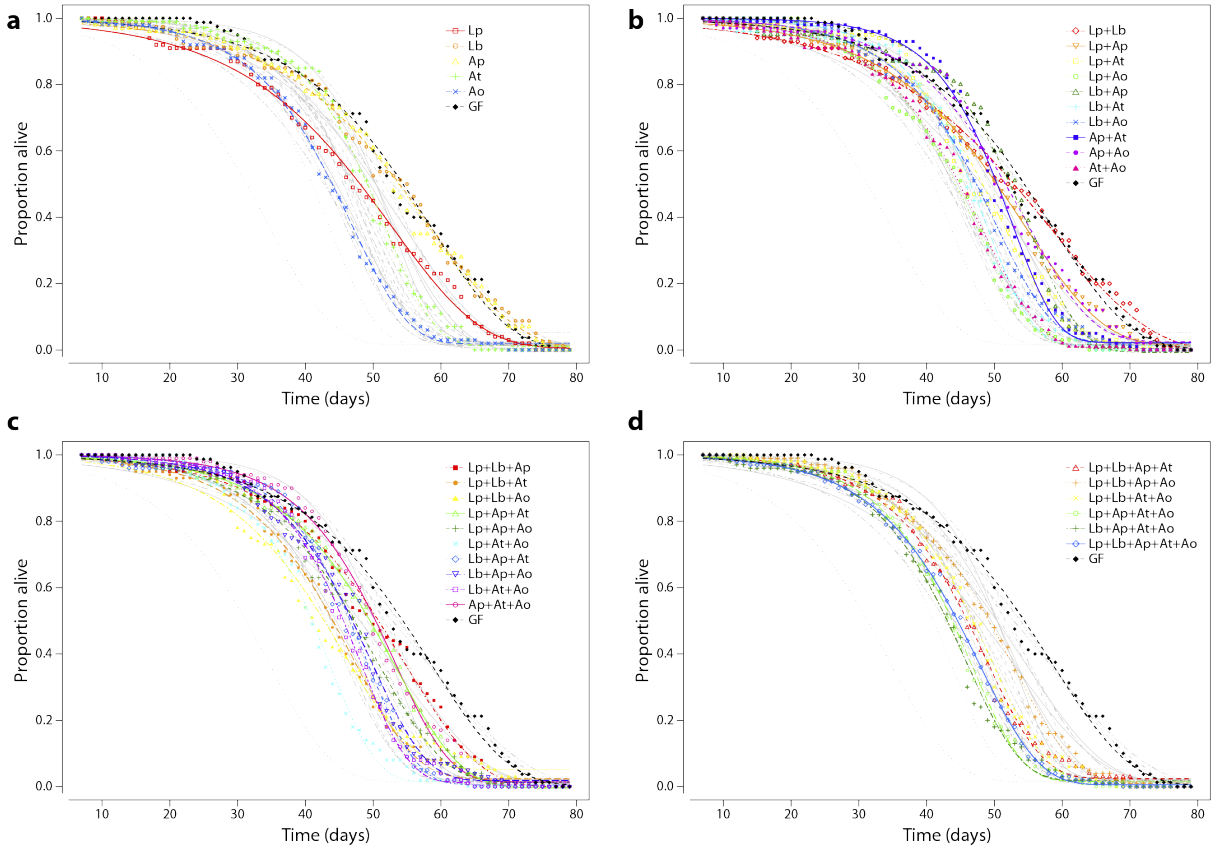

Figure S10. Curve fits to raw lifespan data aggregated from all 5 experimental replicates for each bacterial combination. Curve fits to a 2-parameter Gompertz distribution are depicted (see Methods). Bacterial combinations are grouped by the number of species. (**a**) Single species and germ-free flies. (**b**) Species pairs and germ-free flies. (**c**) Species trios and germ-free flies. (**d**) Species 4-way combinations, 5-way combination, and germ-free flies. All [grayscale] curves are kept as a reference.

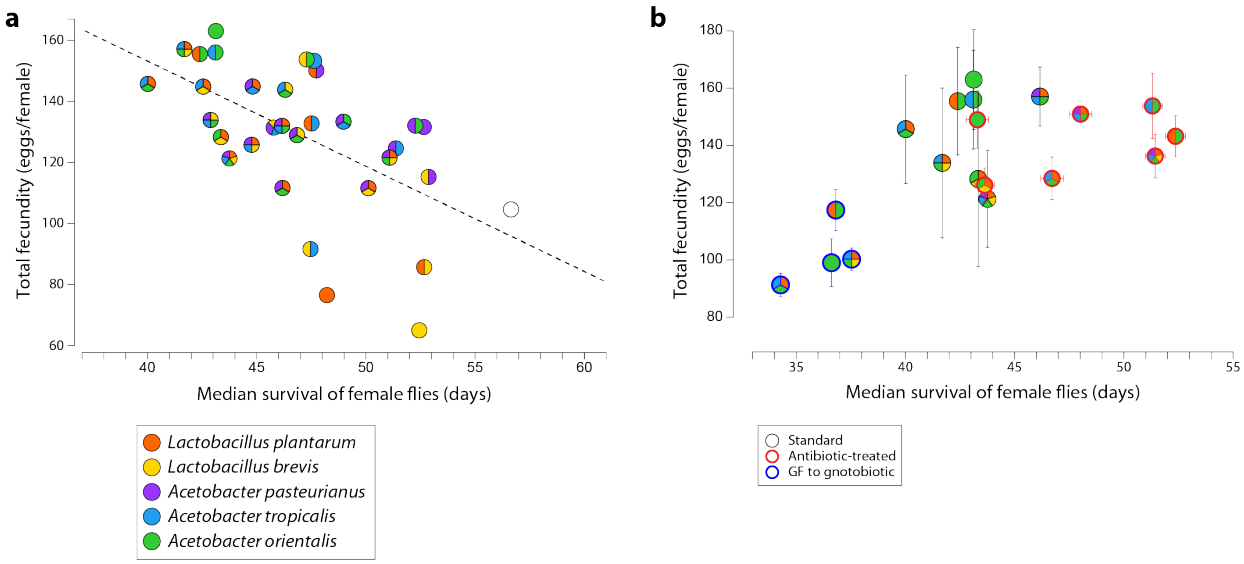

Figure S11. A fitness tradeoff exists between lifespan and fecundity. (**a**) In agreement with prior reports, higher fecundity is associated with shorter lifespan. This tradeoff is apparent for average daily fecundity as well as total fecundity per female. The scatter plot is based on the data from Fig. 2b-c for only female flies. (**b**) The lifespan fecundity tradeoff can be broken by putting flies on antibiotics after their peak reproduction (dots = data from Fig. 2b-c; red circles = gnotobiotic flies were treated with antibiotics (see Methods) after 21 days of reproduction, which encompasses the natural peak fecundity. Note the shifts in lifespan between the regular treatment, the antibiotic treatment, and the late-life bacterial inoculation treatment. Lifespan was significantly extended whereas total fecundity stayed high. Shifting germ-free flies to gnotobiotic treatment after 21 days of life decreased the lifespan without achieving higher reproduction. n=100 flies per treatment for 'original' and 'antibiotic.' n=60 flies per treatment for 'gnotobiotic.'

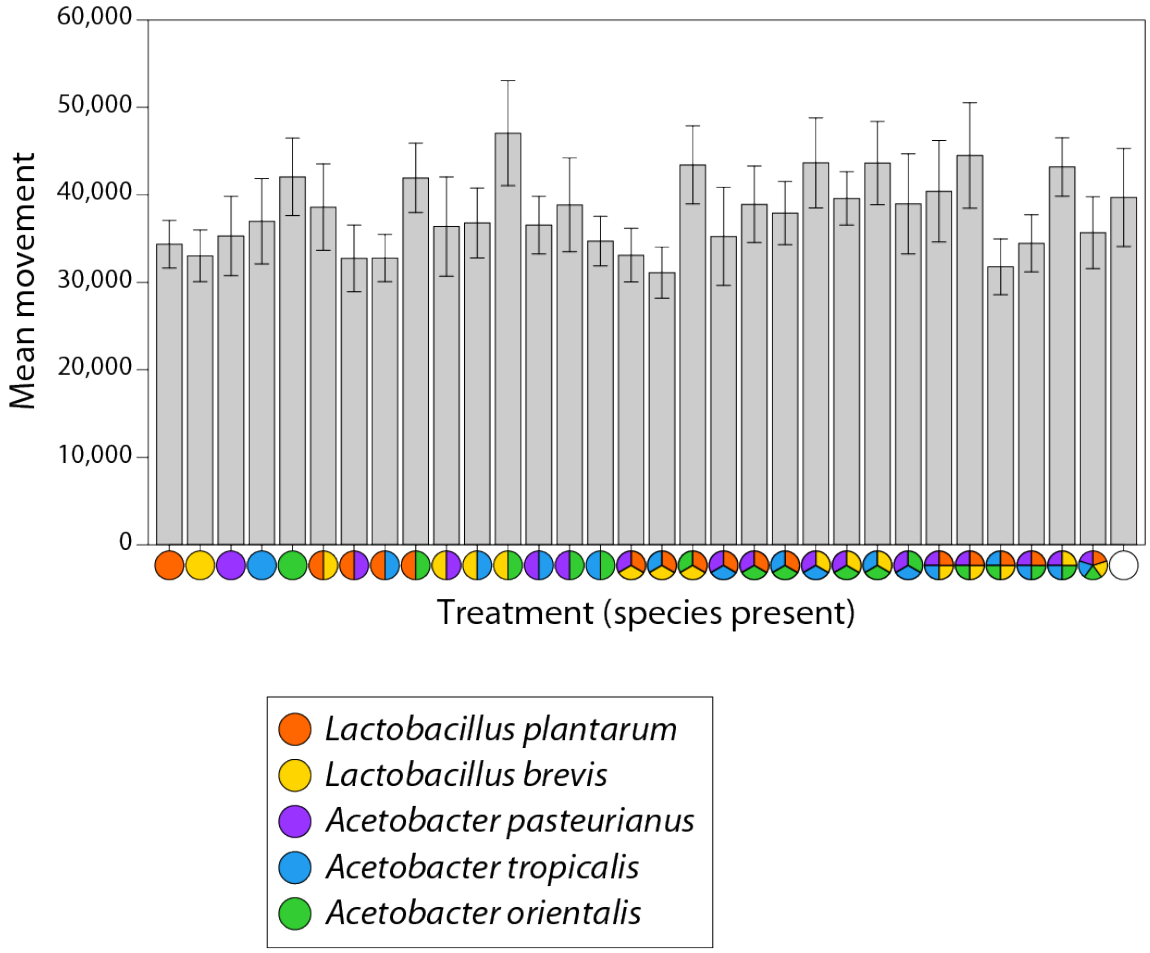

Figure S12. Average fly activity is unrelated to the fitness phenotypes. Fly movement is associated with overall metabolism, including food intake and energy expenditure. To search for behavior changes underlying the physiological differences in our bacterial treatments, we examined changes in fly motility for each bacterial treatment (n=32) in 5 replicate trials (n=20 flies per trial) using the LAMS (Trikinetics) population-based motility assay. Trials were carried out for 7 days. Flies were flipped into fresh vials and placed in the activity monitoring device. The first 24 hours of data were removed to allow for fly acclimation to the new vial. Overall, we found no significant differences between bacterial combinations nor were there any correlations in the mean values with the other physiological data.

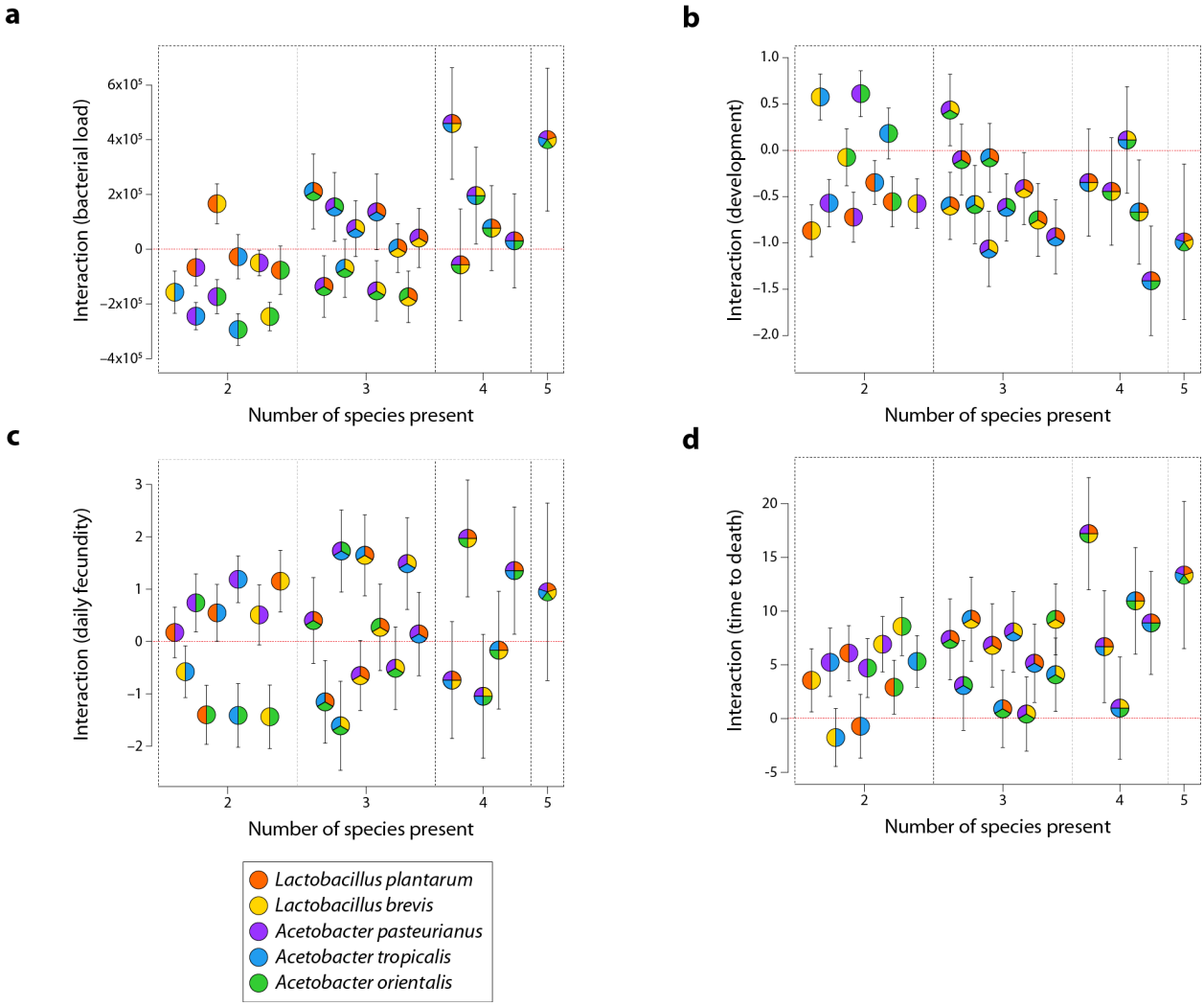

Figure S13. Standard interactions calculated for each phenotype in Fig. 2 and depicted in Fig. 3a-d. Labeling style matches Fig. 2. Error bars are the propagated error from the raw phenotypes.

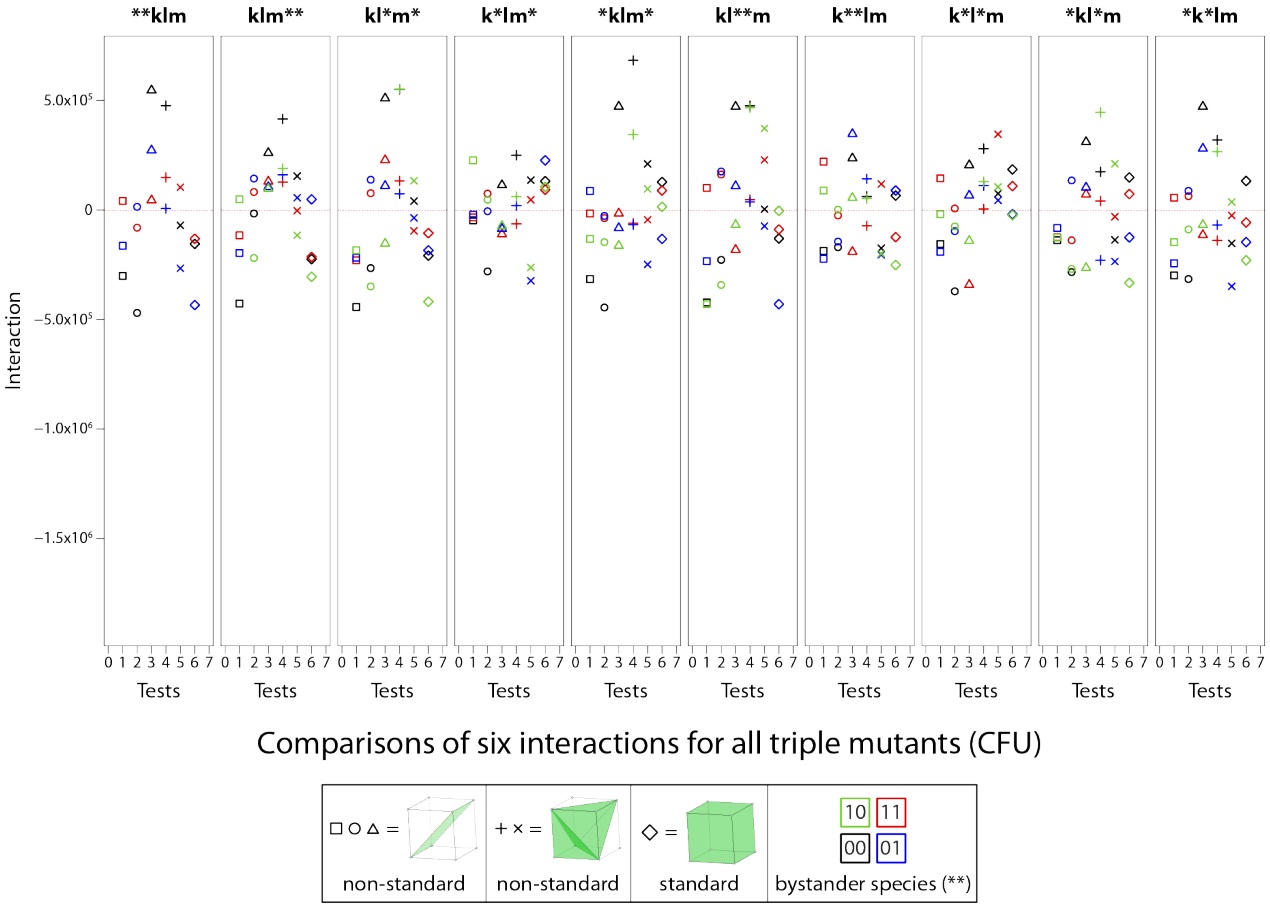

Figure S14. Detailed comparisons of the standard three-way interaction versus the related non-standard tests that incorporate w_{111} and w_{000} for total CFU counts. Interactions on the total bacterial load in flies between sets of three species (equations *g*=square, *i*=circle, *k*=triangle, *m*=plus, *n*=ex ('x'), and u_{111}=diamond) in Math Supplement) are compared to determine (i) whether additive non-standard tests can describe cases of non-additive standard tests and (ii) whether context of other species changes interactions. Each of the 10 combinations of three species (denoted in panel titles as "k", "l", and "m") is compared along with the four variants of bystander species (denoted in the panel titles as "*", and shown by the different colored symbols). The lack of correlation between the colors indicates that bystanders change interactions. As an example of an additive non-standard test explaining a non-additive standard test, see the second panel from the left, "klm**". Here, k=Lp, l=Lb, and m=Ap. Note that the black diamond (standard test) is negative, but the black circle (equation *i*) is roughly zero, indicating that if we consider the Lb bacterial load and the load of the combination with Lp and Ap together, they are equal to the load in flies with the bacterial combination of Lp+Lb+Ap.

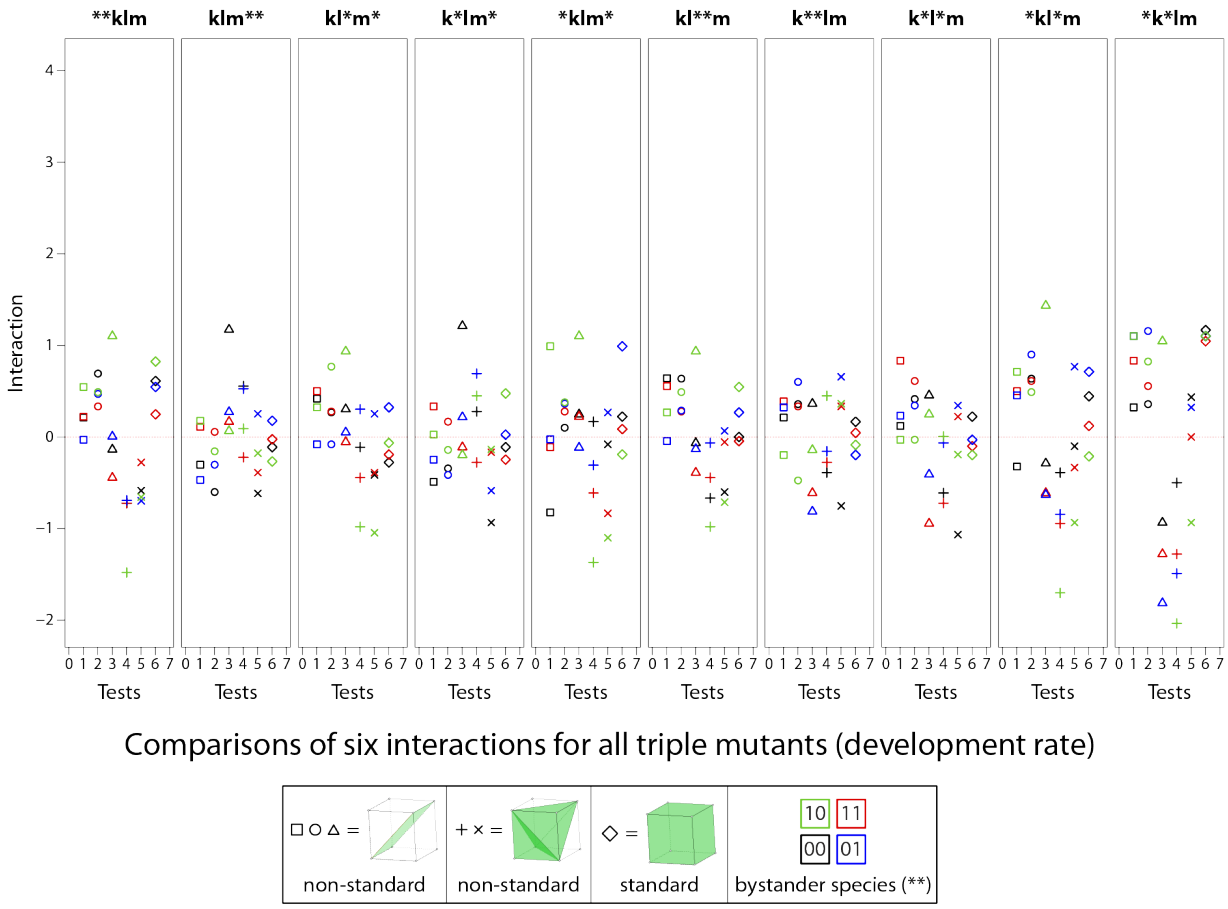

Figure S15. Detailed comparisons of the standard three-way interaction versus the related non-standard tests that incorporate w_{111} and w_{000} for development rate data. Interactions on the total bacterial load in flies between sets of three species (equations *g*=square, *i*=circle, *k*=triangle, *m*=plus, *n*=ex ('x'), and u_{111}=diamond) in Math Supplement) are compared to determine (i) whether additive non-standard tests can describe cases of non-additive standard tests and (ii) whether context of other species changes interactions. Each of the 10 combinations of three species (denoted in panel titles as "k", "l", and "m") is compared along with the four variants of bystander species (denoted in the panel titles as "*", and shown by the different colored symbols).

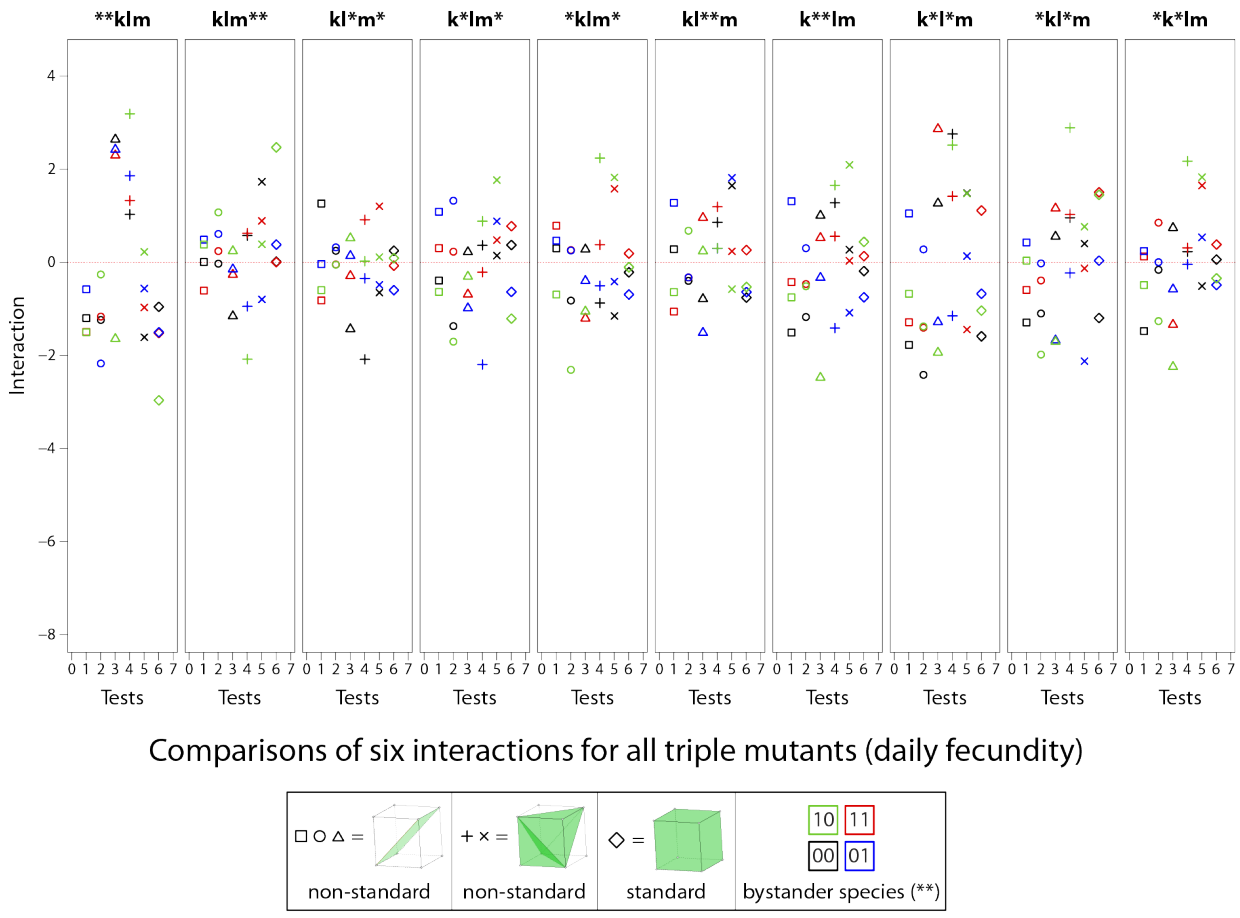

Figure S16. Detailed comparisons of the standard three-way interaction versus the related non-standard tests that incorporate w_{111} and w_{000} for mean daily fecundity data. Interactions on the total bacterial load in flies between sets of three species (equations *g*=square, *i*=circle, *k*=triangle, *m*=plus, *n*=ex ('x'), and u_{111}=diamond) in Math Supplement) are compared to determine (i) whether additive non-standard tests can describe cases of non-additive standard tests and (ii) whether context of other species changes interactions. Each of the 10 combinations of three species (denoted in panel titles as "k", "l", and "m") is compared along with the four variants of bystander species (denoted in the panel titles as "*", and shown by the different colored symbols).

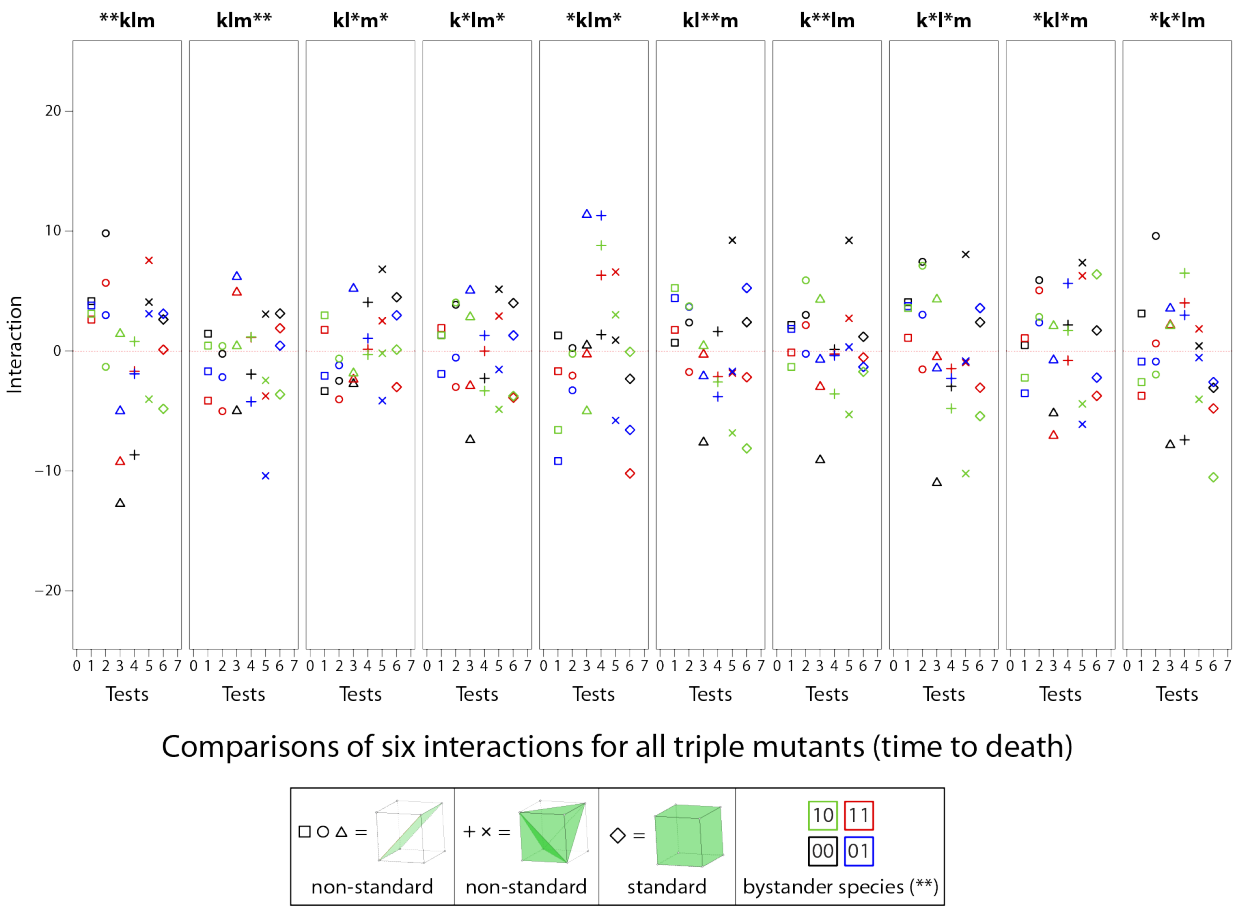

Figure S17. Detailed comparisons of the standard three-way interaction versus the related non-standard tests that incorporate w_{111} and w_{000} for mean lifespan data. Interactions on the total bacterial load in flies between sets of three species (equations *g*=square, *i*=circle, *k*=triangle, *m*=plus, *n*=ex ('x'), and u_{111}=diamond) in Math Supplement) are compared to determine (i) whether additive non-standard tests can describe cases of non-additive standard tests and (ii) whether context of other species changes interactions. Each of the 10 combinations of three species (denoted in panel titles as "k", "l", and "m") is compared along with the four variants of bystander species (denoted in the panel titles as "*", and shown by the different colored symbols).

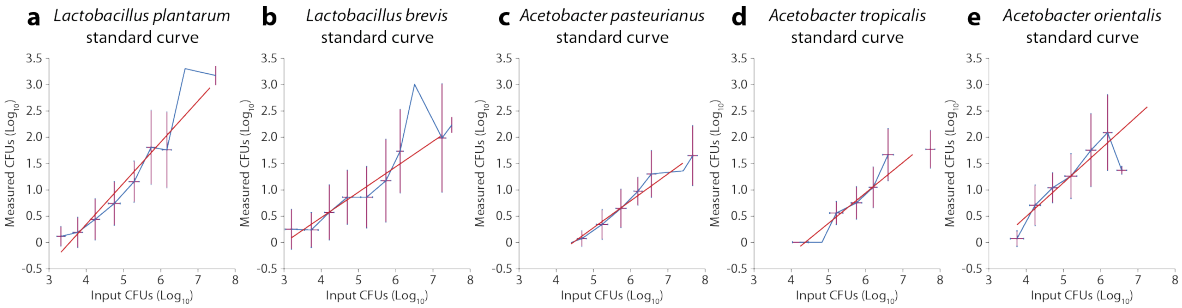

Figure S18. Standard curves used to calculate total CFUs from colony counts (Fig S1, S7). A standard curve was constructed by plating known concentrations of bacteria on selective media with a 96-pin replicator as in *Bacterial load counts* (Methods). Counts were fit to a power law curve using custom scripts in MATLAB.

References

1 Smith, M. I. *et al.* Gut microbiomes of Malawian twin pairs discordant for kwashiorkor. *Science* **339**, 548-554, doi:10.1126/Science.1229000 (2013).

2 Leitão-Gonçalves, R. *et al.* Commensal bacteria and essential amino acids control food choice behavior and reproduction. *PLoS Biology* **15**, e2000862, doi:10.1371/journal.pbio.2000862.s013 (2017).

3 Steinfeld, H. M. Length of life of Drosophila melanogaster under aseptic conditions. *Dissertation thesis*, 1-23 (1927).

4 Smith, P. *et al.* Regulation of life span by the gut microbiota in the short-lived African turquoise killifish. *eLife* **6**, doi:10.7554/eLife.27014 (2017).

5 Martinson, V. G., Douglas, A. E. & Jaenike, J. Community structure of the gut microbiota in sympatric species of wild Drosophila. *Ecology Letters* **26**, 32, doi:10.1111/ele.12761 (2017).

6 Ng, K. M. *et al.* Microbiota-liberated host sugars facilitate post-antibiotic expansion of enteric pathogens. *Nature* **502**, 96-99, doi:10.1038/nature12503 (2014).

7 Coyte, K. Z., Schluter, J. & Foster, K. R. The ecology of the microbiome: Networks, competition, and stability. *Science (New York, NY)* **350**, 663-666, doi:10.1126/science.aad2602 (2015).

8 Sze, M. A. & Schloss, P. D. Looking for a Signal in the Noise: Revisiting Obesity and the Microbiome. *mBio* **7**, doi:10.1128/mBio.01018-16 (2016).

9 Beerenwinkel, N., Pachter, L. & Sturmfels, B. Epistasis and shapes of fitness landscapes. *Statistica Sinica* (2007).

10 Bordenstein, S. R. & Theis, K. R. Host Biology in Light of the Microbiome: Ten Principles of Holobionts and Hologenomes. *PLoS Biology* **13**, e1002226, doi:10.1371/journal.pbio.1002226 (2015).

11 Grilli, J., Barabás, G., Michalska-Smith, M. J. & Allesina, S. Higher-order interactions stabilize dynamics in competitive network models. *Nature*, 1-5, doi:10.1038/nature23273 (2017).

12 Ceja-Navarro, J. A. *et al.* Gut microbiota mediate caffeine detoxification in the primary insect pest of coffee. *Nature Communications* **6**, 1-9, doi:10.1038/ncomms8618 (2015).

13 Brune, A. Symbiotic digestion of lignocellulose in termite guts. *Nature reviews Microbiology* **12**, 168-180, doi:10.1038/nrmicro3182 (2014).

14 Dill-McFarland, K. A., Breaker, J. D. & Suen, G. Microbial succession in the gastrointestinal tract of dairy cows from 2 weeks to first lactation. *Scientific Reports*, 1-12, doi:10.1038/srep40864 (2017).

15 Schieber, A. M. P. *et al.* Disease tolerance mediated by microbiome E. coli involves inflammasome and IGF-1 signaling. *Science (New York, NY)* **350**, 558-563, doi:10.1126/science.aac6468 (2015).

16 Cho, I. & Blaser, M. J. Applications of Next-Generation Sequencing: The human microbiome: at the interface of health and disease. *Nature reviews Genetics* **13**, 260-270, doi:10.1038/nrg3182 (2012).

17 Degnan, P. H., Taga, M. E. & Goodman, A. L. Vitamin B12 as a Modulator of Gut Microbial Ecology. *Cell metabolism* **20**, 769-778, doi:10.1016/j.cmet.2014.10.002 (2014).

18 Seth, E. C. & Taga, M. E. Nutrient cross-feeding in the microbial world. *Frontiers in microbiology* **5**, 350, doi:10.3389/fmicb.2014.00350 (2014).

19 Rolig, A. S., Parthasarathy, R., Burns, A. R., Bohannan, B. J. M. & Guillemin, K. Individual Members of the Microbiota Disproportionately Modulate Host Innate Immune Responses. *CHOM* **18**, 613-620, doi:10.1016/j.chom.2015.10.009 (2015).

20 Ryu, J. H. *et al.* Innate immune homeostasis by the homeobox gene caudal and commensal-gut mutualism in Drosophila. *Science* **319**, 777-782, doi:10.1126/science.1149357 (2008).

21 Wong, C. N. A., Ng, P. & Douglas, A. E. Low-diversity bacterial community in the gut of the fruitfly Drosophila melanogaster. *Environmental Microbiology* **13**, 1889-1900, doi:10.1111/j.1462-2920.2011.02511.x (2011).

22 Chandler, J. A., Lang, J. M., Bhatnagar, S., Eisen, J. A. & Kopp, A. Bacterial communities of diverse Drosophila species: ecological context of a host-microbe model system. *PLoS genetics* **7**, e1002272, doi:10.1371/journal.pgen.1002272 (2011).

23 Newell, P. D. & Douglas, A. E. Interspecies Interactions Determine the Impact of the Gut Microbiota on Nutrient Allocation in Drosophila melanogaster. *Applied and Environmental Microbiology* **80**, 788-796, doi:10.1128/AEM.02742-13 (2013).

24 Obadia, B. *et al.* Probabilistic Invasion Underlies Natural Gut Microbiome Stability. *Current biology : CB* **27**, 1999-2006.e1998, doi:10.1016/j.cub.2017.05.034 (2017).

25 Friedman, J., Higgins, L. M. & Gore, J. Community structure follows simple assembly rules in microbial microcosms. *Nature Publishing Group* **1**, 1-7, doi:10.1038/s41559-017-0109 (2017).

26 May, R. M. Will a large complex system be stable? *Nature* **238**, 413-414 (1972).

27 Paine, R. T. Food-web analysis through field measurement of per capita interaction strength. *Nature*, 1-3 (1992).

28 Vega, N. M. & Gore, J. Stochastic assembly produces heterogeneous communities in the Caenorhabditis elegans intestine. *PLoS Biology* **15**, e2000633, doi:10.1371/journal.pbio.2000633.s012 (2017).

29 Travers, L. M., Garcia-Gonzalez, F. & Simmons, L. W. Live fast die young life history in females: evolutionary trade-off between early life mating and lifespan in female Drosophila melanogaster. *Scientific Reports*, 1-7, doi:10.1038/srep15469 (2015).

30 Yamada, R., Deshpande, S. A., Bruce, K. D., Mak, E. M. & Ja, W. W. Microbes Promote Amino Acid Harvest to Rescue Undernutrition in Drosophila. *Cell reports* **10**, 865-872, doi:10.1016/j.celrep.2015.01.018 (2015).

31 Blum, J. E., Fischer, C. N., Miles, J. & Handelsman, J. Frequent Replenishment Sustains the Beneficial Microbiome of Drosophila melanogaster. *mBio* **4**, e00860-00813-e00860-00813, doi:10.1128/mBio.00860-13 (2013).

32 Fischer, C. *et al.* Metabolite exchange between microbiome members produces compounds that influence Drosophila behavior. *eLife* **6**, doi:10.7554/eLife.18855 (2017).

33 Clark, R. I. *et al.* Distinct Shifts in Microbiota Composition during Drosophila Aging Impair Intestinal Function and Drive Mortality. *CellReports*, 1-13, doi:10.1016/j.celrep.2015.08.004 (2015).

34 Chippindale, A. K., Leroi, A. M., Kim, S. B. & Rose, M. R. Phenotypic plasticity and selection in Drosophila life-history evolution. I. Nutrition and the cost of reproduction *Journal of evolutionary biology*, 1-23 (1993).

35 Leslie, P. H. On the use of matrices in certain population mathematics. *Biometrika* **33**, 183-212 (1945).

36 Ramalho, M. O., Bueno, O. C. & Moreau, C. S. Species-specific signatures of the microbiome from Camponotus and Colobopsis ants across developmental stages. *PLOS ONE* **12**, e0187461, doi:10.1371/journal.pone.0187461.s010 (2017).

37 Kwong, W. K. *et al.* Dynamic microbiome evolution in social bees. *Science Advances* **3**, e1600513, doi:10.1126/sciadv.1600513 (2017).

38 Brucker, R. M. & Bordenstein, S. R. The Hologenomic Basis of Speciation: Gut Bacteria Cause Hybrid Lethality in the Genus Nasonia. *Science (New York, NY)* **341**, 667-669, doi:10.1126/science.1240659 (2013).

39 Moeller, A. H. *et al.* Cospeciation of gut microbiota with hominids. *Science (New York, NY)* **353**, 380-382, doi:10.1126/science.aaf3951 (2016).

40 Moran, N. A. & Sloan, D. B. The Hologenome Concept: Helpful or Hollow? *PLoS Biology* **13**, e1002311, doi:10.1371/journal.pbio.1002311.g001 (2015).

41 Faith, J. J. *et al.* The long-term stability of the human gut microbiota. *Science (New York, NY)* **341**, 1237439, doi:10.1126/science.1237439 (2013).

Math Supplement: Mathematical Framework for Detecting Microbiome Interactions in the Host

December 12, 2017

Contents

1 Pairwise Species Interactions (Figure 1)

Data Collection For each of the 32 fully combinatorial experiments in which flies are constantly fed defined bacteria on their food, we collect the mean CFU abundance for each of the 24 individual fly samples by averaging the three technical replicates for each sample. For each experiment, the median of these *sample CFU counts* may be taken to obtain *median CFU counts* (we use the median rather than the mean because the CFU count data is quite variable). The raw data are displayed in Figure S1.

Pairwise correlations (Figure 1b) The diversity of an experiment is the number of bacterial species that are provided on the food. For the set of experiments that have a given diversity N, we compute the pairwise correlation between bacteria i and j in the following way. For the subset of experiments of diversity N with microbes i and j, the sample CFU counts for i and j for each experiment are aggregated. Then, we calculate the Spearman's rank correlation coefficient of these pairs of data, and arrive at a pairwise correlation value between species i and j that is between -1 (ordinal CFU counts between the species are perfectly anticorrelated) and 1 (perfectly correlated). This process is repeated for each species pairing to build a pairwise correlation matrix for each diversity.

Pairwise interactions (Figure 1c) We infer the species interactions by assuming that the system obeys the generalized Lotka-Volterra equations,

$$\frac{d}{dt}x_i = x_i\left(\mu_i + \sum_{j=1}^{N} M_{ij}x_j\right),$$

and by assuming that the median CFU counts of each experiment are at equilibrium. At equilibrium, the time derivative on the left hand side vanishes, and we assume that the steady state is non-trivial (i.e. $x_i \neq 0$); if we call the steady state of each microbe for a given experiment $\tilde{x}_i$, then an experiment of diversity N will correspond to N algebraic equations of the form

$$0 = \mu_i + \sum_{j=1}^{N} M_{ij}\tilde{x}_j.$$

If there are M experiments of diversity N, then there are MN equations that must be simultaneously satisfied. We consider a "low-diversity" group that groups diversities 1 and 2 together (which consists of $1*5+2*10=25$ equations), and a "high-diversity" group that groups diversities 3, 4, and 5 together (which consists of $3*10+4*5+5*1=55$ equations). For each of these groups, we can rewrite these linear equations in matrix form as $0 = A\vec{x}$, where A is made up of the $\tilde{x}_i$ and $\vec{x} = [M_{11}, M_{12}, \ldots, M_{55}, \mu_1, \ldots, \mu_5]^T$. We assume $\mu_i = 1$ to obtain a nonzero result for M, which effectively absorbs the growth rates μ_i into the interaction values M_{ij}. We solve this system of equations for $\vec{x}$ with linear least-squares, since the linear system using the high-diversity group is overdetermined. The solution to this least-squares problem is the interaction matrix M, which we plot as a food web in Figure 1c.

Pairwise interactions (Figure S2a,b) Paine [2] presented a direct calculation of interaction strength, which we used to validate the overall trends we observed as a function of diversity. To measure the effect of a single species on the other species in a community, Paine removed the single species of interest and measured the resulting changes in abundance of the remaining species. The interaction strength is calculated as

$$\frac{treatmentCFUs - controlCFUs}{controlCFUs},$$

where $treatmentCFUs$ is the median species abundance with the species of interest absent and $controlCFUs$ is the median abundance when it is present [2]. To be clear, the CFU abundances in the equation are both (*treatment* and *control*) for the same species, while the removal is for a second species. Thus, an asymmetric matrix of interactions is calculated. Using the combinatorial experiments where each species has been removed and, in each removal, each remaining species has been quantified, allows us to measure the complete set of pairwise interactions for the cases where diversity goes from two to one species (Figure S2a) and from five to four species (Figure S2b) by removing one species at a time. We display the asymmetric matrices for the N=1,2 and N=4,5 cases as directed graphs.

Determining statistical trends For the four correlation matrices and the two interaction matrices, we show that both the correlations and the interactions become more negative at higher diversities. To achieve this, we compare the same matrix element across different diversities using the non-parametric Kendall rank correlation coefficient. Each matrix element is ranked according to its size over increasing diversities,

resulting in an ordinal vector of length 4 for the correlation matrix and of length 2 for the interaction matrix. Through the Kendall rank correlation coefficient, the ranking for each matrix element is compared to a strictly increasing vector ([1, 2, 3, 4] or [1, 2] for the two respective cases), resulting in a τ coefficient that is between -1 and 1. For the correlation matrices there are 10 such τ coefficients with a mean of -0.4 (corresponding to all possible pairings of 5 bacteria), and for the interaction matrices there are 25 τ coefficients with a mean of -0.44 (since interactions need not be symmetric, and self-interactions occur as well). The matrices becoming more negative at higher diversities would correspond to negative τ coefficients. To determine whether the distribution of τ coefficients is significantly more negative than a distribution centered at 0, we apply the Wilcoxon signed-rank test. The resulting one-sided p-values for the correlation matrices and interaction matrices are 0.0323 and 0.0139, indicating that there is a significant trend in the values of both the correlation and interaction matrices to decrease. When we assume that undetected species have an abundance of 1000 CFUs, corresponding to the limit of detection, the resulting one-sided p-values were 0.0323 (unchanged) for correlation matrices and 0.0359 for interaction matrices, indicating the results are robust to changes in CFUs below the limit of detection.

2 Introduction to Geometric Interactions (Figure 3)

For an n-genotype system, higher order genetic interactions are commonly described in terms of interaction coordinates and related forms see [5]. For example, marginal and conditional epistasis are formulas obtained with this approach, where we test the effect of one set of loci on the interactions between other sets of loci. Interaction might also include circuits, see [5] for details. Besides a graspable biological interpretation, circuits also have a geometric interpretation, as these are formulas whose terms can be parametrized by certain sets of vertices on an n-cube and where n is the number of loci considered. This geometric interpretation is particularly useful, as it facilitates the parametrization of these types of formulas. Different sets of vertices in an n-cube then yield different circuits. In general, however, it is an open problem to determine all circuits in an n-cube, resp. in an n-genotype system, as the number increases dramatically with n, see [7] where the 4-dimensional case has been considered. Moreover, there is not a clear biological interpretation of all possible circuits of the n-cube.

In this work, we exploit the geometry of the 5-cube in terms of lower dimensional cubes and lift well known lower rank interactions to the higher dimensional space. For instance, we test whether the positive interaction between Ap and Lp stays positive when At is introduced. Clearly, with this approach we only examine a subset of all possible interactions, but the ones we find are interpretable and comparable with other studies (e.g. Newell and Douglas 2014 [3]). Moreover, we believe that our approach is simple enough to be scalable to higher dimensions. In the following, we explain how this approach generalizes to n-dimensional systems and to all lower rank interactions inside this system, and we give examples of how the mathematical approach applies to other biological systems specifically to bacterial interactions in the gut microbiome.

3 Glossary for interactions - Mathematical Terminology

The terminology we use in this work is an adaptation of the wording used in genetics to the study of interactions among bacterial species in fruit flies. For convenience we include the following intuitive definitions of terms we will repeatedly use later on:

- **n-species system**: a system of n types of bacterial species in the microbiome (present or absent).
- **n-cube (n dimensional unit hypercube)**: is an n-dimensional generalization of a square (2-cube) and three dimensional cube whose sides have unit lengths. When n=5 the 5-cube has 32 vertices, 80 edges, 80 square faces, 40 3-cubes and 10 4-cubes, see [1].
- **Interaction coordinates**: are basis elements for the interaction spaces associated to a system consisting of n-bacterial species (or an n-cube). Interaction coordinates are given by linear combinations of phenotypes associated to all combinations of species in the n-species system.
- **Circuits**: are certain linear combinations of interaction coordinates.

- **Triangulation**: is the local shape of the fitness landscape imposed by the phenotypes of neighboring genotypes (see Box 1a for an example).
- **Standard interactions (or standard tests)**: are 2, 3, 4 and 5-way interactions on all pairs, triples, quadruples and five tuples of species leaving the remaining species absent.
- **Non-standard interaction (or non-standard tests)**: higher-order interactions arising as a generalization of the standard test, interaction coordinates for the 3 and 4 and 5 species systems as well as circuits for the 3 species case, and by allowing the species not present to be occupied by bystanders, whose presence/absence is constant across the species considered in the standard test.

In this work, we will focus on a 5 species system consisting of 32 bacterial combinations. We encode the different bacterial combinations by a binary string S of lengths 5. Each entry of such a string S represents a bacterial species isolated inside a number of flies guts. For instance, S=00000 describes the germ-free fly, S=11111 describes the fly colonized with all 5 species of bacteria. With this binary notion, each bacterial combination also defines a vertex of a 5-dimensional cube G. Together with the 5-cube G, we also consider the following four phenotypes associated with the bacterial combinations: bacterial load (CFUs), development rate, fecundity, and time to death. These phenotypes associated with each bacterial combination in binary notation are denoted simply by w_S. The order of the bacterial species and the specific bacterial loads are summarized in Table 1.

Table 1: **The 32 different bacterial loads.**

4 Interaction space

In this section, we recall the notion of interaction coordinates and circuits (for the three cube) first defined in [5]. We first describe these spaces abstractly for arbitrary values of n. In a second part, we describe how one can recursively extend these formulas to define new interaction formulas in higher dimensional settings.

4.1 Interaction coordinates

Let $i = i_1, i_2, \ldots, i_n$ be a vertex of an n-dimensional cube with at least two coordinates i_j, i_k being 1. The interaction coordinates u_i can be defined (up to a scalar) in the following way:

$$u_{i_1,i_2,\ldots,i_n} := \frac{1}{2^n - 1} \sum_{j_1=0}^{1} \sum_{j_2=0}^{1} \cdots \sum_{j_n=0}^{1} (-1)^{i_1 j_1 + i_2 j_2 + \cdots + i_n j_n} w_{j_1 j_2 \ldots j_n} \tag{1}$$

where w_- are values of a corresponding phenotypes and indexed by the vertices of the n-dimensional cube. It then follows, that there are $2^n - n - 1$ interaction coordinates. Moreover, these coordinates are linearly independent and form a vector space basis of the interaction space.

In genetics, interaction coordinates are also called marginal epistasis in [5].

4.2 Circuits

Linear combinations of interaction coordinates might give rise to circuits. In the following, the only circuits we will consider are the ones previously presented in the 3-dimensional setting in [5]. In formulas, these

circuits can be presented as follows:

$$\begin{aligned}
a &:= u_{110}+u_{111}=w_{000}-w_{010}-w_{100}+w_{110}\\
b &:= u_{110}-u_{111}=w_{001}-w_{011}-w_{101}+w_{111}\\
c &:= u_{101}+u_{111}=w_{000}-w_{001}-w_{100}+w_{101}\\
d &:= u_{101}-u_{111}=w_{010}-w_{011}-w_{110}+w_{111}\\
e &:= u_{011}+u_{111}=w_{000}-w_{001}-w_{010}+w_{011}\\
f &:= u_{011}-u_{111}=w_{100}-w_{101}-w_{110}+w_{111}\\
g &:= u_{110}+u_{101}=w_{000}-w_{011}-w_{100}+w_{111}\\
h &:= u_{110}-u_{101}=w_{001}-w_{010}-w_{101}+w_{110}\\
i &:= u_{110}+u_{011}=w_{000}-w_{010}-w_{101}+w_{111}\\
j &:= u_{110}-u_{011}=w_{001}-w_{011}-w_{100}+w_{110}\\
k &:= u_{101}+u_{011}=w_{000}-w_{001}-w_{110}+w_{111}\\
l &:= u_{101}-u_{011}=w_{010}-w_{011}-w_{100}+w_{101}
\end{aligned}$$

$$\begin{aligned}
m &:= -u_{011}-u_{101}-u_{110}-u_{111}=w_{001}+w_{010}+w_{100}-w_{111}-2w_{000}\\
n &:= -u_{011}-u_{101}-u_{110}+u_{111}=w_{011}+w_{101}+w_{110}-w_{000}-2w_{111}\\
o &:= u_{011}+u_{101}-u_{110}-u_{111}=w_{010}+w_{100}+w_{111}-w_{001}-2w_{110}\\
p &:= u_{011}+u_{101}-u_{110}+u_{111}=w_{000}+w_{011}+w_{101}-w_{110}-2w_{001}\\
q &:= u_{011}-u_{101}+u_{110}-u_{111}=w_{001}+w_{100}+w_{111}-w_{010}-2w_{101}\\
r &:= u_{011}-u_{101}+u_{110}+u_{111}=w_{000}+w_{011}+w_{110}-w_{101}-2w_{010}\\
s &:= -u_{011}+u_{101}+u_{110}+u_{111}=w_{000}+w_{101}+w_{110}-w_{011}-2w_{100}\\
t &:= -u_{011}+u_{101}+u_{110}-u_{111}=w_{001}+w_{010}+w_{111}-w_{100}-2w_{011}.
\end{aligned}$$

Biological and geometric interpretations of these circuits follow from the descriptions given in [5, §.3] for the genetic setting.

4.3 Recursively constructing higher order interactions

We now describe how interaction coordinates in lower dimensional cubes and the circuits a-t extend to interaction formulas in higher dimensional cubes.

For instance, the two-way interaction

$$u_{11}=w_{00}+w_{11}-w_{01}-w_{10}$$

extends to the following $80=10\cdot 2^3$ different interaction formulas in a five species system:

$$\begin{aligned}
\alpha_{**klm} &= w_{00klm}+w_{11klm}-w_{01klm}-w_{10klm}\\
\alpha_{*k*lm} &= w_{0k0lm}+w_{1k1lm}-w_{0k1lm}-w_{1k0lm}\\
\alpha_{*kl*m} &= w_{0kl0m}+w_{1kl1m}-w_{0kl1m}-w_{1kl0m}\\
\alpha_{*klm*} &= w_{0klm0}+w_{1klm1}-w_{0klm1}-w_{1klm0}\\
\alpha_{k**lm} &= w_{k00lm}+w_{k11lm}-w_{k01lm}-w_{k10lm}\\
\alpha_{k*l*m} &= w_{k0l0m}+w_{k1l1m}-w_{k0l1m}-w_{k1l0m}\\
\alpha_{k*lm*} &= w_{k0lm0}+w_{k1lm1}-w_{l0lm1}-w_{k1lm0}\\
\alpha_{kl**m} &= w_{kl00m}+w_{kl11m}-w_{kl01m}-w_{kl10m}\\
\alpha_{kl*m*} &= w_{kl0m0}+w_{kl1m1}-w_{kl0m1}-w_{kl1m0}\\
\alpha_{klm**} &= w_{klm00}+w_{klm11}-w_{klm01}-w_{klm10},
\end{aligned}\tag{2}$$

where $**$ indicates two out of five loci. The remaining loci k,l,m are then either wild or 1, and all possible 2^3 combinations are allowed. Interactions of this type where considered for the five locus case in [5, §.7].

Similarly, one extends to the five species system the four interaction coordinates $u_{111},\ u_{110}, u_{011}, u_{101}$ defined by (1) above in the following fashion:

$$\beta_{***kl} = \sum_{j_1=0}^{1}\sum_{j_2=0}^{1}\sum_{j_3=0}^{1}(-1)^{*j_1+*j_2+*j_3}w_{j_1j_2j_3kl}$$

$$\beta_{**k*l} = \sum_{j_1=0}^{1}\sum_{j_2=0}^{1}\sum_{j_4=0}^{1}(-1)^{*j_1+*j_2+*j_4}w_{j_1j_2kj_4l}$$

$$\beta_{**kl*} = \sum_{j_1=0}^{1}\sum_{j_2=0}^{1}\sum_{j_5=0}^{1}(-1)^{*j_1+*j_2+*j_5}w_{j_1j_2klj_5}$$

$$\beta_{*k*l*} = \sum_{j_1=0}^{1}\sum_{j_3=0}^{1}\sum_{j_5=0}^{1}(-1)^{*j_1+*j_3+*j_5}w_{j_1kj_3lj_5}$$

$$\beta_{*kl**} = \sum_{j_1=0}^{1}\sum_{j_4=0}^{1}\sum_{j_5=0}^{1}(-1)^{*j_1+*j_4+*j_5}w_{j_1klj_4j_5}$$

$$\beta_{k*l**} = \sum_{j_2=0}^{1}\sum_{j_4=0}^{1}\sum_{j_5=0}^{1}(-1)^{*j_2+*j_4+*j_5}w_{kj_2lj_4j_5}$$

$$\beta_{kl***} = \sum_{j_3=0}^{1}\sum_{j_4=0}^{1}\sum_{j_5=0}^{1}(-1)^{*j_3+*j_4+*j_5}w_{klj_3j_4j_5}$$

$$\beta_{*k**l} = \sum_{j_1=0}^{1}\sum_{j_3=0}^{1}\sum_{j_4=0}^{1}(-1)^{*j_1+*j_3+*j_4}w_{j_1kj_3j_4l}$$

$$\beta_{k**l*} = \sum_{j_2=0}^{1}\sum_{j_3=0}^{1}\sum_{j_5=0}^{1}(-1)^{*j_2+*j_3+*j_5}w_{kj_2j_3lj_5}$$

$$\beta_{k***l} = \sum_{j_2=0}^{1}\sum_{j_3=0}^{1}\sum_{j_4=0}^{1}(-1)^{*j_2+*j_3+*j_4}w_{kj_2j_3j_4l}.$$

As before, the notation $***$ indicates three loci out of five. The remaining loci k, l are assumed to be fixed and either $kl = 00, kl = 01, kl = 11$ or $kl = 10$. Moreover, the sums are taken over integer numbers between 0 and 1.

Given these extended interaction coordinates also allows us to extend the circuits *a-t* to the five species setting. To do this, it is enough to consider the circuit formulas *a-t* given above, and replace the u_{i_1,i_2,i_3} with the corresponding extended interaction coordinates. The biological and geometric interpretation of these interaction formulas can easily be deduced from the lower dimensional ones (given in [5] for the three species case).

Similarly one also extends the $2^4 - 5 = 11$ interaction coordinates $u_{i_1,\ldots,i_4}$ defined by equation (1) and $n = 4$.

5 Two disjoint families of interactions

In the following, we are interested in comparing the outcomes of two disjoint families of interaction formulas in the five bacterial species setting. The first family is smaller in size and consists of the standard interactions. These involve a variety of different combinations of bacterial species, without involving excessively many computations per test.

The second family (non-standard interactions) consists of a large number of different interaction formulas recursively defined. These interactions are more accurate in describing the interaction of the bacterial combinations under inspections and depend on the presence of the bystanders [5].

These two families of interactions we consider in this work are new and inspired by [6] and [4] (the second reference for standard tests).

5.1 Standard interactions

Consider the two species interaction formula, given by:

$$u_{11} = w_{00} + w_{11} - w_{01} - w_{10}$$

where w_{00} indicates a phenotype, such as daily fecundity, time to death, CFU or development rate, associated to the (empty) bacterial combination 00, and similarly for w_{11}, w_{01} and w_{10}. Biologically, the meaning of this interaction formula is well understood: it compares the phenotype contributions of the wild and double mutant with the phenotype contributions of the single mutants. Geometrically, the summands of u_{11}, w_{00}, w_{11}, w_{01} and w_{10}, are indexed by the four vertices of a unital square.

We then consider the following generalizations of u_{11} for the 3-, 4- and 5-species system:

$$u_{111} = w_{000} + w_{011} + w_{101} + w_{110} - w_{100} - w_{010} - w_{001} - w_{111}$$

$$\begin{aligned} u_{1111} = {} & w_{0000} + w_{1100} + w_{0110} + w_{0011} + w_{1010} + w_{0101} + w_{1001} + w_{1111} \\ & - w_{1000} - w_{0100} - w_{0010} - w_{0001} - w_{1011} - w_{1101} - w_{0111} - w_{1110} \end{aligned}$$

$$\begin{aligned} u_{11111} = {} & w_{00000} - w_{00001} - w_{00010} - w_{00100} - w_{01000} - w_{10000} + w_{11000} \\ & + w_{10100} + w_{10010} + w_{10001} + w_{01100} + w_{01010} + w_{01001} + w_{00110} \\ & + w_{00101} + w_{00011} - w_{11100} - w_{11010} - w_{11001} - w_{10110} - w_{10101} \\ & - w_{10011} - w_{01110} - w_{01101} - w_{01011} - w_{00111} + w_{11110} + w_{11101} \\ & + w_{11011} + w_{10111} + w_{01111} - w_{11111}. \end{aligned}$$

In the following, we simply call u_{11} the 2-way interaction, u_{111} the 3-way interaction, u_{1111} the 4-way interaction, and u_{11111} the 5-way interaction. From the given formulas it is clear that these interactions are defined by 4, 8, 16, and 32 terms, respectively. The signs change according to the definition of the interaction coordinate function given in equation (1). Biologically, one can say that each such 3, 4 and 5-way interaction compares the contribution of phenotypes when an even number of bacterial combinations (equivalent to mutations) were inserted versus contributions of phenotypes measured when an odd numbers of bacterial combinations have been inserted (e.g. w_{00} and w_{11} vs w_{01} and w_{10}).

From the 2-way interaction above one deduces a further 10 two-way interactions in a five species system by considering two loci and leaving the remaining three loci not mutated (i.e. the remaining bacterial species are not present). The three-way interaction gives rise to 10 further three-way interactions of this type, arising by considering three loci and letting the remaining ones not mutated. Similarly, the four-way interaction yields 5 similar four-way interactions by letting the remaining species absent. Together, this approach gives:

$$\binom{5}{2} + \binom{5}{3} + \binom{5}{4} + \binom{5}{5} = 26 \tag{3}$$

different higher order interactions in a five species system, which we call standard interactions. All of these standard interactions compare certain phenotype contributions indexed by an even number of bacteria species present, versus an odd number of bacteria species present. The number of standard interactions we found in Equation (3) matches the results of [4].

To summarize, the standard interactions involving two loci in a five species system are:

$$\begin{aligned}
u_{00**0} &= w_{00000} + w_{00110} - w_{00010} - w_{00100} \\
u_{**000} &= w_{00000} + w_{11000} - w_{01000} - w_{10000} \\
u_{*0*00} &= w_{00000} + w_{10100} - w_{00100} - w_{10000} \\
u_{0**00} &= w_{00000} + w_{01100} - w_{00100} - w_{01000} \\
u_{*00*0} &= w_{00000} + w_{10010} - w_{00010} - w_{10000} \\
u_{0*0*0} &= w_{00000} + w_{01010} - w_{00010} - w_{01000} \\
u_{00*0*} &= w_{00000} + w_{00101} - w_{00001} - w_{00100} \\
u_{*000*} &= w_{00000} + w_{10001} - w_{00001} - w_{10000} \\
u_{0*00*} &= w_{00000} + w_{01001} - w_{00001} - w_{01000} \\
u_{000**} &= w_{00000} + w_{00011} - w_{00001} - w_{00010}
\end{aligned}$$

These u-interactions arise from the 2-way interaction and always involve two species (indicated with $*$) out of five leaving the other three species absent. Geometrically, these u-interactions involve the four vertices of certain square faces inside a 5-dimensional cube G.

The standard interactions, which involve three species out of five, will be denoted by u and are obtained from the 3-way interaction. These u-interactions involve the eight vertices of the specified cubes inside G:

$$\begin{aligned}
u_{00***} &= w_{00000} + w_{00011} + w_{00101} + w_{00110} - w_{00100} - w_{00010} - w_{00001} - w_{00111} \\
u_{***00} &= w_{00000} + w_{01100} + w_{10100} + w_{11000} - w_{10000} - w_{01000} - w_{00100} - w_{11100} \\
u_{**0*0} &= w_{00000} + w_{01010} + w_{10010} + w_{11000} - w_{10000} - w_{01000} - w_{00010} - w_{11010} \\
u_{*0**0} &= w_{00000} + w_{00110} + w_{10010} + w_{10100} - w_{10000} - w_{00100} - w_{00010} - w_{10110} \\
u_{0***0} &= w_{00000} + w_{00110} + w_{01010} + w_{01100} - w_{01000} - w_{00100} - w_{00010} - w_{01110} \\
u_{**00*} &= w_{00000} + w_{01001} + w_{10001} + w_{11000} - w_{10000} - w_{01000} - w_{00001} - w_{11001} \\
u_{*00**} &= w_{00000} + w_{00011} + w_{10001} + w_{10010} - w_{10000} - w_{00010} - w_{00001} - w_{10011} \\
u_{*0*0*} &= w_{00000} + w_{00101} + w_{10001} + w_{10100} - w_{10000} - w_{00100} - w_{00001} - w_{10101} \\
u_{0**0*} &= w_{00000} + w_{00101} + w_{01001} + w_{01100} - w_{01000} - w_{00100} - w_{00001} - w_{01101} \\
u_{0*0**} &= w_{00000} + w_{00011} + w_{01001} + w_{01010} - w_{01000} - w_{00010} - w_{00001} - w_{01011}
\end{aligned}$$

The following five standard interactions arise from the 4-way interaction described by u_{1111} above and involve four species out of the five, leaving out the remaining bacterial community:

$$\begin{aligned}
u_{****0} &= w_{00000} + w_{11000} + w_{01100} + w_{00110} + w_{10100} + w_{01010} + w_{10010} + w_{11110} \\
&\quad - w_{10000} - w_{01000} - w_{00100} - w_{00010} - w_{10110} - w_{11010} - w_{01110} - w_{11100} \\
u_{***0*} &= w_{00000} + w_{11000} + w_{01100} + w_{00101} + w_{10100} + w_{01001} + w_{10001} + w_{11101} \\
&\quad - w_{10000} - w_{01000} - w_{00100} - w_{00001} - w_{10101} - w_{11001} - w_{01101} - w_{11100} \\
u_{**0**} &= w_{00000} + w_{11000} + w_{01010} + w_{00011} + w_{10010} + w_{01001} + w_{10001} + w_{11011} \\
&\quad - w_{10000} - w_{01000} - w_{00010} - w_{00001} - w_{10011} - w_{11001} - w_{01011} - w_{11010} \\
u_{*0***} &= w_{00000} + w_{10100} + w_{00110} + w_{00011} + w_{10010} + w_{00101} + w_{10001} + w_{10111} \\
&\quad - w_{10000} - w_{00100} - w_{00010} - w_{00001} - w_{10011} - w_{10101} - w_{00111} - w_{10110} \\
u_{0****} &= w_{00000} + w_{01100} + w_{00110} + w_{00011} + w_{01010} + w_{00101} + w_{01001} + w_{01111} \\
&\quad - w_{01000} - w_{00100} - w_{00010} - w_{00001} - w_{01011} - w_{01101} - w_{00111} - w_{01110}
\end{aligned}$$

Geometrically, these interactions involve the 16 vertices of the specified 4-cubes inside G. The last standard

interaction is simply given by the following expression involving all five species and all 32 fitness values:

$$\begin{aligned} u_{*****} &= u_{11111} \\ &= w_{00000} - w_{00001} - w_{00010} - w_{00100} - w_{01000} - w_{10000} + w_{11000} \\ &+ w_{10100} + w_{10010} + w_{10001} + w_{01100} + w_{01010} + w_{01001} + w_{00110} \\ &+ w_{00101} + w_{00011} - w_{11100} - w_{11010} - w_{11001} - w_{10110} - w_{10101} \\ &- w_{10011} - w_{01110} - w_{01101} - w_{01011} - w_{00111} + w_{11110} + w_{11101} \\ &+ w_{11011} + w_{10111} + w_{01111} - w_{11111}. \end{aligned}$$

Geometrically, this interaction involves all vertices of G. In Figure 1 below we highlight the regions delimited by the vertices defining the 26 standard interactions described above inside a projection of a five cube G. In all cases, the sign (+ or −) of the summand (i.e. the phenotype being added) is defined by the the number of bacterial species involved.

For example, in a three bacterial system consisting of the following 8 bacterial combinations $G = \{000, 001, 010, 100, 110, 011, 101, 11\}$ there are three standard interactions involving two out of three species:

$$\begin{aligned} u_{**0} &= w_{000} + w_{110} - w_{100} - w_{010} \\ u_{*0*} &= w_{000} + w_{101} - w_{100} - w_{001} \\ u_{0**} &= w_{000} + w_{011} - w_{010} - w_{001} \end{aligned}$$

together with the 3-way interaction u_{111}, described above.

5.2 Non-standard interactions

In the following, we compare the results of these standard tests with the corresponding non-standard tests in a five species system. By this we mean all the interactions we described in Section 4 which are different from the standard interaction formulas described in Section 5.1. Thus, non-standard tests are higher-order interactions arising by allowing the species not present under the standard test, circuits and interaction coordinates to be occupied by bystanders, whose presence/absence is constant across the species considered in the standard test. It follows that non-standard tests measure how the context of additional species change the interaction effects.

The standard tests and non-standard tests we consider in this work are examples of the more generally defined marginal and conditional interactions in genetics context. To specify the species we condition on and to differentiate among types of conditional interactions, we refrain from using this terminology.

We computed 910 different non-standard interactions and 26 different standard interactions. From Section 4 and the recursive nature of the five dimensional cube, it follows that the non-standard interactions we inquire have a well understood biological and geometric interpretation.

Finally, we note that despite the formulas describing non-standard and standard interactions all being different, the two sets of interactions are not statistically independent as they use the same underlying data sets.

5.3 Significance testing of interactions

In order to decide whether an interaction is non-zero, we took the uncertainty in the phenotype measurements into account and devised a statistical test as follows. Since the phenotype measurements come with their standard errors, we computed the corresponding propagation of error for each interaction (standard and non). This error was determined by taking the square root of the sum of squares of the standard errors involved in each interaction formula. For example, for u_{11}, the propagated standard error $s(u_{11})$ is

$$s(u_{11}) = \sqrt{s_{00}^2 + s_{11}^2 + s_{01}^2 + s_{10}^2}$$

where s_{00} denotes the standard error of w_{00}, etc.

Moreover, if different formulas give rise to the same interaction term, we considered only the formula yielding the smallest propagation error, that is, the formula involving the least number of operations. For

instance, each interaction term $a, \ldots, t$ can be defined in two ways, one involving a difference between interaction coordinates and a direct way. The direct way involves less operations, and therefore a smaller propagation error.

We then determined significant interactions in the following way. We assumed that each interaction formula comes from a Gaussian distribution with mean 0 and standard deviation given by the computed propagation error. For each interaction u, we performed a two-sided null hypothesis test. The null hypothesis states that the true value of the interaction is $u = 0$, versus the alternative hypothesis that $u \neq 0$. We then considered an interaction statistically significant if the p-value was below 0.05. This means, that if the null hypothesis was true, the probability of obtaining the result of the interaction u we computed would be 5%.

In total, we tested 936 interactions (26 standard tests plus 910 non-standard tests). To account for the multiple comparisons, we corrected all p-values using the Benjamini-Hochberg procedure in order to control the false discovery rate at 5%; that is, we eventually considered an interaction statistically significant if the corrected p-value was below 0.05.

6 Supplemental Results of Interaction Testing

In this section we summarize the main findings we obtained through the computations described above. In the first part, we focus on the smaller family of higher-order interactions and on the second part we compare the outcomes of these interactions with non-standard interactions. In the last part, we focus on specific standard and non-standard interactions which compare the wild type and the triple mutants in different ways.

6.1 Results for standard interactions

To summarize the results of the standard interactions presented above we average the results of the standard 2-, 3-, 4- and 5-way tests. Thus, we let a_2 be the sum of all standard 2-way interactions u_{**} divided by the number of 2-way standard interactions (which is 10). Similarly, for a_3, a_4 and a_5.

Term	**CFU**	**dev**	**fd**	**td**
a_2	-117000	-0.235	-0.0524	4.09
a_3	8920	-0.472	0.175	5.44
a_4	141000	-0.552	0.274	8.95
a_5	400000	-0.990	0.948	13.4

Table 2: **The terms** $a_2, \ldots, a_5$ for the four phenotypes of fecundity per day (fd), CFU, time to death (td) and development rate (dev).

From Table 2 we deduce that in average the interaction tends to increase with the number of terms in the standard formulas. We also note that the sign of the interaction (positive or negative) is already determined by the sign of the average 2- and 3-way interaction. This means that when the average contribution of the two (or three) species combinations is higher than the average contribution of the single species combinations, also the average contribution of an even number of species is higher than the average contribution of an odd number of species (regardless of how many even or odd species are considered 2,4,8,16) as determined by the standard tests for interactions. Together with the results of Table 2, we also consider the average interactions of the standard 2-,3-, 4- and 5-way interactions normalized by the number of present bacterial species. That is $n_2 = a_2/2$,$n_3 = a_3/3$, $n_4 = a_4/4$ and $n_5 = a_5/5$, see Table 3 for the corresponding results.

Term	CFU	dev	fd	td
n_2	-58531	-0.117	-0.026	2.043
n_3	18288.333	-0.169	0.034	2.035
n_4	35312.5	-0.138	0.069	2.236
n_5	80094	-0.198	0.190	2.671

Table 3: **The terms** $n_2, \ldots, n_5$ for the four phenotypes of fecundity per day (fd), CFU, time to death (time d) and development rate (dev).

It is clear from examining the average interaction values (i.e. the terms $a_2, \ldots, a_5$) that the total contribution increases as the number of species increases. However, when we normalize these average values to the number of species, we see a more constant contribution for each individual species, see Table 3.

Thus, if interactions quantify the degree to which we can predict the phenotype of the microbiome when a new species is added, overall the microbiome is less predictable as we add additional species. However, on a per-species basis, the degree of unpredictability stays constant. And if we consider the number of combinations, the unpredictability decreases. Thus, while our analysis indicates that the microbiome problem increases in complexity as more species are added, there is reason for hope. For instance, if we discover a rule that determines *a priori* which non-standard test will be additive (versus showing interaction), the predictability of the microbiome will increase as we add species. However, our fundamental conclusion is that the relationships between species rather than the species themselves produce increasingly complex interactions. Therefore, our efforts at building a predictable framework should focus on the interactions between species as much as on the interactions between the individual species themselves.

To this point, when we compare the distributions of the raw data with the results of the standard interactions, we see that linear trends in the raw data do not necessary translate to the same trends in the standard interaction data (Figure S6). For example, consider time to death: the raw data indicates that increasing the number of bacterial species results in a decrease in the time to death. However, the standard tests indicate that interaction tends to increase with the number of loci involved (see Table 2), and hence with the numbers of terms in the standard interaction formulas. Finally, from the data in the Fig. S13, we deduce that the above observations remain valid by considering the (fewer) significant standard interactions rather than all standard interactions (Figure S6). For completeness, we also computed Pearson's correlation coefficients on all 26 standard interactions, and on the raw CFUs, development rate, daily fecundity, time to death data. See Table 4. The tests in bold in Table 4 which reached significance level ($p < 0.05$) are time to death versus CFUs with a p-value of 0.0011. We also see that the correlation might change sign when passing from the raw data to the computed standard interactions (as it is, for example, for time to death vs development rate).

	CFU	Development rate	Daily fecundity	Time to death
CFU	-	**-0.46** (p=0.0082)	0.14 (p=0.4516)	**-0.55** (p=0.0011)
Development rate	-0.38 (p=0.0523)	-	-0.34 (p=0.0558)	0.35 (p=0.0502)
Daily fecundity	0.13 (p=0.5403)	**-0.46** (p=0.0178)	-	**-0.45** (p=0.0103)
Time to death	0.10 (p=0.6222)	**-0.49** (p=0.0120)	**0.43** (p=0.0290)	-

Table 4: **Pearson's correlation coefficients and significance level for all 26 standard interactions and raw data**. Below the diagonal, we indicate Pearson's correlation coefficients and the corresponding p-values for all standard tested interactions (26 samples), similarly above the diagonal for the raw data (32 data points).

6.2 Results for all computed interactions

In this section, we describe the results contained in Fig. 3 and Fig. S6 in the main text, obtained while computing the 910 non-standard interactions together with 26 standard interactions for the phenotypes of CFU, development rate, daily fecundity, time to death. As main findings we showed that there are many significant positive and negative interactions among bacterial species in fruit flies. Moreover, among all

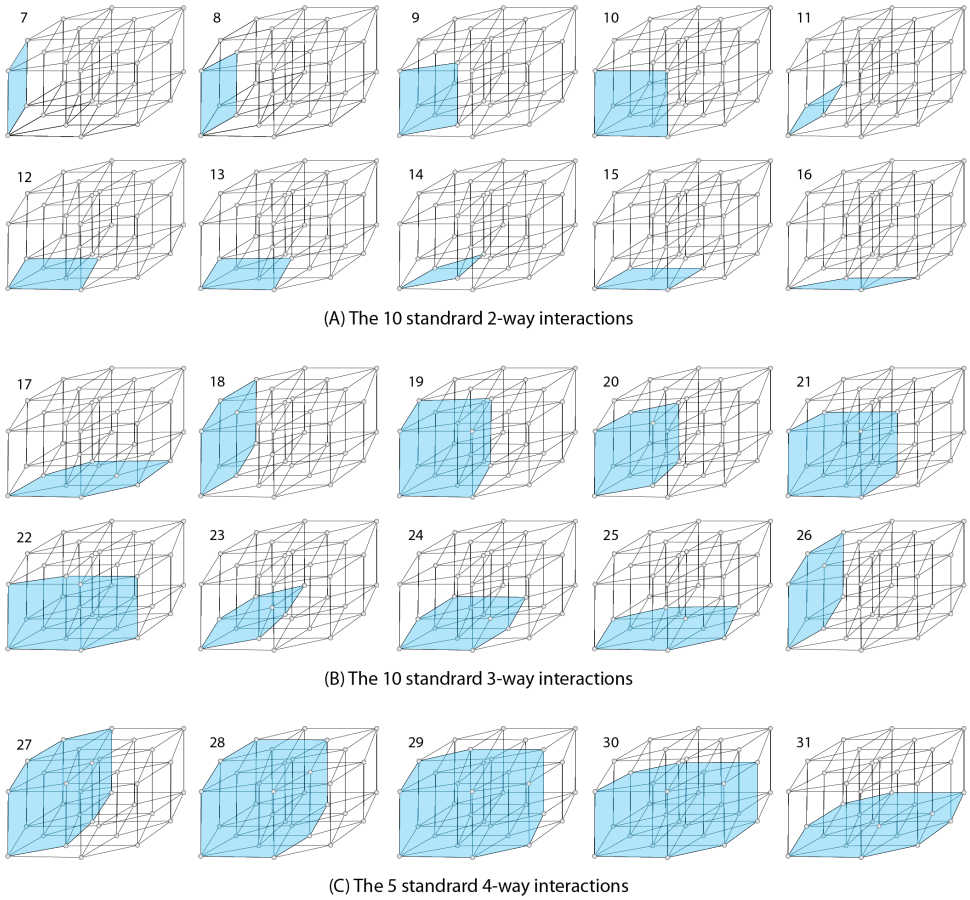

Figure 1: **Geometric description of the 26 standard interactions**. The highlighted regions inside the projections of the 5-dimensional cube indicate the vertices involved in the corresponding interaction. The interaction u_{11111} is defined by all 32 vertices and therefore omitted.

intricate ways bacterial species interact with each other we found that for some phenotypes (CFUs and daily fecundity) the standard interactions essentially fully capture interaction trends measured also by the non-standard interactions. However, for development rate and time to death we found that many new significant interactions arise under mixing procedures which cannot be quantified by the standard tests alone. Moreover, comparing the correlation Table 4 with Table 6 we found correlated interactions between phenotypes where neither the raw measurements nor the standard tests were correlated. More results, on all the computed correlations are in Figure S6 (main text).

The coefficients a_i and n_j for all non-standard interactions are then as indicated in the following Table 5. The average contributions of the circuit interactions vanish and are hence omitted in the table.

Term	**CFU**	**dev**	**fd**	**td**
a_2	-49672.063	0.050	-0.023	0.211
a_3	-92665.250	0.158	-0.210	0.763
a_4	-176164.545	0.170	-0.376	1.492
a_5	-250353.846	0.147	-0.400	3.252
n_2	-12418.016 0.025	-0.011	0.053	
n_3	-11583.156	0.012	-0.006	0.095
n_4	-11010.284	0.011	-0.024	0.093
n_5	–8075.931	0.005	- 0.013	0.105

Table 5: The columns *dev* indicates the coefficients for development rate, *daily fecundity* for daily fecundity and $time_d$ for time to death.

Finally, we underpin the above findings by testing if the two probability distributions corresponding to standard and non-standard interactions come from the same continuous distributions. Since standard tested and non-standard tests are computed from the same underlying data, and are therefore statistically dependent, to test the difference between the distributions we performed a two-sample and two-sided Kolmogorov-Smirnov (KS) test. The results of the KS test for the phenotypes of CFU (D = 0.2011, p-value = 0.2583) and daily fecundity (D = 0.13407, p-value = 0.7539) indicate that there is little evidence to reject the null-hypothesis of STD tests and non-STD tests coming from the same distributions. On the other hand, the results of the KS test for the phenotypes of development rate (D = 0.45934, p-value = $4.661 \cdot 10^{-05}$) and time to death (D = 0.50769, p-value = $4.384 \cdot 10^{-06}$) suggest that it is unlikely that the STD tests and non-STD tests come from the same distributions.

	CFU	**Development**	**Daily fecundity**	**Time to death**
CFU	-	**-0.18** ($p < 0.0005$)	**0.16** ($p < 0.0005$)	**-0.32** ($p < 0.0005$)
Development	**-0.67** ($p < 0.0005$)	-	**-0.35** ($p < 0.0005$)	**-0.14** ($p < 0.0005$)
Daily fecundity	**0.52** ($p < 0.0005$)	**-0.85** ($p < 0.0005$)	-	**-0.24** ($p < 0.0005$)
Time to death	**-0.70** ($p < 0.0670$)	**-0.34** (p= 0.0104)	**-0.75** ($p < 0.0005$)	-

Table 6: **Pearson's correlation coefficients and significance level for all tested interactions**. Below the diagonal, we indicate Pearson's correlation coefficients and the corresponding p-values for statistically significant interactions ($p < 0.05$ after multiple testing correction, between 27 and 78 pairwise complete comparisons). Similarly, above the diagonal we compute correlations for all non-standard tested interactions regardless of statistical significance (910 data points).

6.3 Comparisons for the triple mutants

In this section, we explain how interactions involving all 10 three-species combinations in a five species system behave under mixing, see Fig. S14-S17 in the main text. More specifically, to obtain these figures we consider the circuits g, i, k, m, n and the interaction coordinate u_{111}. We then lifted these interactions to the five species system, as described in Section 4.3. In particular, in this way, we obtained that each such interaction yields 40 interactions in the five species system (as $\binom{5}{3} = 10$ and there are 4 choices for the bystanders). In each figure (Fig. S14-S17 in the main text) we focused on one phenotype (CFU, development

rate, daily fecundity or time to death). In each plot we represented with the same color the six interactions corresponding to g, i, k, m, n and u_{111}. The different colors then reflect the state of the bystanders: black if the bystanders are both 00, red if the bystanders are both mutated, and blue (resp. green) if only one bystander is mutated.

7 Discussion of Interaction Coordinates

Consistently, we see that the same interaction coordinates have correlated values across the different phenotypes that we measured. A simple explanation is that the rich microbial interactions underlying these phenotypes affect some central aspect of fly physiology that is reflected in multiple life history traits.

With the goal of quantifying higher order interactions we computed various interaction formulas. We also extracted a set of 26 interaction formulas (which we called standard interactions) and compared them with the results of 910 (different) interaction formulas. We found that for certain phenotypes the standard interactions approximate well the distribution of the other more involved computations. Since the number of all possible interactions is large, and unknown in general, it is important to find a more parsimonious approach based on fewer interactions that still capture the main interaction signals. This is particularly advisable since the number of all possible interactions increases with the number of loci and the relative contributions coming from each test are mainly small. Moreover, analyzing smaller sets of particularly expressive and biologically interpretable interactions would not only be computationally more efficient, but also facilitate the comparisons of higher order genetic interactions arising in different biological context (for example infected fruit flies, or fruit flies treated with antibiotics). Moreover, the recursive approach we proposed here to define higher order interaction coordinates, as well as the computations we carried out, easily extends to settings with more loci. Thus, our methodology provides a way to reduce the experimental burden of examining combinatorial interactions in the microbiome. We also observe that our computations are based on discrete data points. But since the nature of the phenotypes we analyzed is continuous, it would be interesting to extend our studies and consider a fitting continuous setting. Finally, our computations and conclusion consider the propagation of uncertainty in phenotype measurements, but it would be interesting to develop a quantitative statistical framework accounting for possible sensible noise in the data set.

8 Supplements

8.1 Data transformation

All the interactions we compute are based on and generalize the additive genetic epistasis formula $u_{11} = w_{00} + w_{11} - w_{01} - w_{10}$. This additive formula relates to the multiplicative formula $m_{11} = w_{00}w_{11} - w_{01}w_{10}$ up to a logarithmic transformation. That is, composing the phenotype with a log transformation, we have:

$$\log(w_{00}) + \log(w_{11}) - \log(w_{01}) - \log(w_{10}) = \log(w_{00}w_{11}) - \log(w_{01}w_{10}).$$

To highlight that the interactions we find do not depend on the additive approach we choose, we computed the same interactions as above also for the logarithmic (in base 2) transformation of the data. With no surprise, the interactions might dependent on the choice of the data transformation. More generally, we conclude by observing that transformations (possibly) depend on the true distribution of the observed (measured) data. Since the true distribution of our measurement remains unknown, we find it more reasonable to present our findings based on the actual measured data.

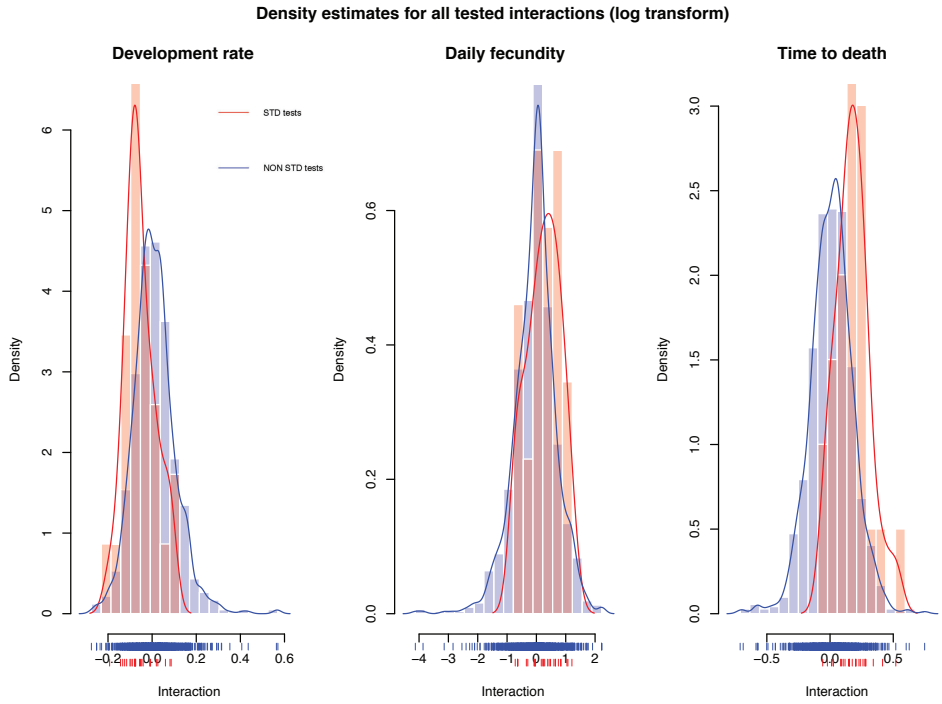

Figure 2: **Density plot of all tested interactions (standard in red and non standard in blue) for the $\log_2$ transformed data.**

References

[1] H.§. M. Coxeter.*Regular Polytopes*, London, Methuen,New York, Pitman 1949. 20-321 (1948)

[2] R. T. Paine *Food-web analysis through field measurement of per capita interaction strength*, Nature 355, 73-75 (1992)

[3] P. D. Newell, A. E. Douglas, *Interspecies Interactions Determine the Impact of the Gut Microbiota on Nutrient Allocation in Drosophila melanogaster*, Appl. Environ. Microbiol, vol. 80 no. 2 788-796 (2014)

[4] J. Grilli, G. Barabs, MJ. Michalska-Smith, S. Allesina, *Higher-order interactions stabilize dynamics in competitive network models*, Nature. 2017 Aug 10;548(7666):210-213. (2017)

[5] N. Beerenwinkel, L. Pachter, B. Sturmfels, *Epistasis and shapes of fitness landscapes* Statistica Sinica 17, 1317-1342 (2007)

[6] N. Beerenwinkel, L. Pachter, B. Sturmfels, SF. Elena and RE. Lenski, *Analysis of epistatic interactions and fitness landscapes using a new geometric approach*, BMC Evolutionary Biology 20077:60 (2007)

[7] P. Huggins, B. Sturmfels, J. Yu, and DS. Yuster. *The Hyperdeterminant and Triangulations of the 4-Cube.* Mathematics of Computation 77, no. 263 (2008)